

1 Timescales and Regions of the Sensitivity of Atlantic
2 Meridional Volume and Heat Transport:
3 Toward Observing System Design

4 Patrick Heimbach¹ *, Carl Wunsch¹, Rui M. Ponte²,
Gael Forget¹, Chris Hill¹, and Jean Utke³

- (1): MIT, EAPS, Cambridge, MA, USA
{heimbach, cwunsch, gforget, cnh}@mit.edu
(2): AER, Lexington, MA, USA
rponte@aer.com
(3): ANL, Chicago, IL, USA
utke@mcs.anl.gov

Revised version, submitted to *Deep Sea Res.*, special issue on the AMOC

Keywords:

meridional overturning circulation; poleward heat transport;
decadal variability; adjoint sensitivities; dual state space;
observing system design; oceanic teleconnections; ...

5 February 4, 2011

*Corresponding author address: Patrick Heimbach; MIT, EAPS room 54-1518; 77 Massachusetts Avenue; Cambridge, MA 02139; USA; Email: heimbach@mit.edu; Phone: 617-253-5259; Fax: 617-253-4464

6	Contents	
7	1 Introduction	4
8	2 The Method	6
9	3 Adjoint Pathways and Processes	8
10	3.1 Atlantic Signatures With Up to 4 Years Propagation Time	9
11	3.2 Amplitude-Weighted Time Scales	12
12	3.3 Zonal and Meridional Sections Through Time	13
13	3.4 Meridional Coherence	15
14	3.5 Meridional Volume Versus Heat Transport	15
15	3.6 Optimized versus Non-optimized Solution	16
16	3.7 Abyssal Processes and Signatures Beyond 10 Years	18
17	3.8 Atmospheric Impacts	19
18	4 Discussion	20
19	4.1 Implications for observing system design	20
20	4.2 Preliminary conclusions	22
21	Appendix: Model configuration	27
22	References	27

Abstract

24 A dual (adjoint) model is used to explore elements of the oceanic state influencing
25 the meridional volume and heat transports (MVT and MHT) in the subtropical North
26 Atlantic so as to understand their variability and to provide the elements of useful
27 observational program design. Focus is on the effect of temperature (and salinity) per-
28 turbations. On short time-scales (months), as expected, the greatest sensitivities are
29 to local disturbances, but as the time scales extend back to a decade and longer, the
30 region of influence expands to occupy much of the Atlantic basin and significant areas
31 of the global ocean, although the influence of any specific point or small area tends to
32 be quite weak. The propagation of information in the dual solution is a clear mani-
33 festation of oceanic teleconnections. It takes place through identifiable “dual” Kelvin,
34 Rossby, and continental shelf-waves with an interpretable physics, in particular in terms
35 of dual expressions of barotropic and baroclinic adjustment processes. Among the no-
36 table features are the relatively fast time scales of influence (albeit weak in amplitude)
37 of influence between 26°N and the tropical Pacific and Indian Ocean, the absence of
38 dominance of the subpolar North Atlantic, significant connections to the Agulhas leak-
39 age region in the southeast Atlantic on time scales of five to ten years, and the marked
40 sensitivity propagation of Doppler-shifted Rossby waves in the Southern Ocean on time
41 scales of a decade and beyond. Regional, as well as time-dependent differences, between
42 MVT and MHT sensitivities highlight the lack of a simple correspondence between their
43 variability. Some implications for observing systems for the purpose of climate science
44 are discussed.

1 Introduction

The need for understanding the physics of change in the ocean and their consequences for the global climate system are producing increasing calls for useful and sustained observing systems capable of quantitative description of the circulation. Useful systems are expensive to create, not easy to deploy and maintain, and *decisions made today about particular system design will largely determine what will be known of the ocean circulation for decades to come*—a major responsibility for those attempting to construct ocean observing systems. Thus, because of the considerable expense, and the long-term consequences, and in contrast with most of the history of physical oceanography, one seeks a better, prior, understanding of the capabilities of any particular system design—before commitments are made to actually deploy it.

The most difficult aspects of observing system design concern the questions of what should be measured, and how well such measurements must be made. By “well” is meant all of the usual considerations of accuracy, precision, sampling rates and space-time coverage underlying any system. Measurement purposes can be widely different. Are systems intended for “monitoring”, “early warning”, or for understanding? Is one concerned with detecting change over months or decades? Answers to these questions must account for cost-benefit ratios and the ease or difficulty of sustaining the system.

Different emphases affect the choice of an observing system. If one were interested in the meridional heat transport (MHT) or volume transport (MVT) at a given latitude in the North Atlantic, then producing a “now-cast” will likely put the focus on measuring variables in the vicinity of the latitude in question (in particular temperature T and meridional velocity v). However, if knowledge of the time history becomes relevant (annual to decadal and beyond) or “early warning” is a focus, it is conceivable that the strongest influence on changes in MHT or MVT will come through remote perturbations of various origins, whose influence superimpose, and whose propagation time scales (advective, wave-like, or diffusive) are relevant to the problem at hand.

The ocean is a fluid with a long memory. Thus changes in any particular variable at any particular location will result from the summation, and interaction, of phenomena potentially having occurred long ago and in remote locations. On long enough time scales, almost any oceanographic quantity of interest has to be considered as part of the global circulation and dynamically connected to it. *Wunsch and Heimbach* [2009] considered regions which dominate global meridional overturning circulation (MOC) variability on decadal time scales. That the ocean can transmit signals and changes over long distances and over extremely

79 long times is well known. Examples are the dynamical calculation of baroclinic adjustment
80 times by *Veronis and Stommel* [1956] and the multi-decadal sea level adjustment time scales
81 discussed by *Johnson and Marshall* [2002], *Cessi et al.* [2004], *Stammer* [2008], among many
82 others. In the context of climate variability the problem has also been framed in terms
83 of global oceanic teleconnections, e.g., *Greatbatch and Peterson* [1996], *Cessi and Otheguy*
84 [2003], *Johnson and Marshall* [2004], *Liu and Alexander* [2007]. The tracer calculations by
85 *Wunsch and Heimbach* [2008] and transit time or age distributions by, e.g., *Holzer and Hall*
86 [2000], *Haine and Hall* [2002], *Khatiwala* [2007], *Haine et al.* [2008], *Primeau and Deleer-*
87 *snijder* [2009] show that adjustment times of the ocean extend to millennial time scales and
88 are completely global in scope.

89 To understand quantitatively the behavior of any regional oceanographic changes (e.g. local
90 heat content, property transports through sections), one needs to know their sensitivity to
91 non-local transients at various times and regions. In this paper, we begin the process of
92 elucidating the space-time structure of the controls on oceanic changes of climate relevance
93 for the purpose of evaluating potential climate observing systems. The basis for these calcu-
94 lations is knowledge of the sensitivity of physical elements of oceanic GCMs to disturbances
95 in both internal and external parameters and based upon the powerful method of an adjoint
96 model.

97 These methods are described in numerous references (e.g., *Marotzke et al.* [1999], *Wun-*
98 *sch* [2006a], *Griewank and Walther* [2008], *Heimbach* [2008]) and are summarized in the
99 Appendix. For present purposes, an adjoint model can be understood as a “dual” GCM,
100 representing the flow of information in the GCM over all space and time scales. Related
101 previous efforts are those of *Marotzke et al.* [1999] who considered a time span of only one
102 year, *Köhl* [2005] who examined Atlantic MOC sensitivities to surface forcing and initial
103 conditions at interannual time scales, and *Bugnion et al.* [2006a,b] whose emphasis was
104 multi-centennial equilibrium estimates. The present focus is on seasonal to decadal time
105 scales of climatologically important elements of the ocean circulation, and their spatial
106 variations, that would influence decisions about the measurement systems necessary to un-
107 derstand their behavior. Although we do not specifically discuss the prediction problem, an
108 implicit assumption is that prediction, if possible, necessitates both adequate understanding
109 and observation of the most sensitive elements.

110 Consider by way of example the total meridional heat and volume transports across 26°N in
111 the North Atlantic. These diagnostics can be computed as zonal ($\int d\theta$) and vertical ($\int dz$)

112 integrals of instantaneous temperature T and meridional velocity v ,

$$\begin{aligned}
 J_{MHT} &= \frac{c_p \rho}{t_f - t_i} \int_{t_i}^{t_f} \int_{\text{depth}} \int_{\text{lon}} v(t) \cdot T(t) \, d\theta \, dz \, dt, & \text{petawatts-PW} \\
 J_{MVT} &= \frac{1}{t_f - t_i} \int_{t_i}^{t_f} \int_{0\text{m}}^{1200\text{m}} \int_{\text{lon}} v(t) \, d\theta \, dz \, dt, & \text{Sverdrups (Sv)-}10^6 \text{m}^3/\text{s}
 \end{aligned}
 \tag{1} \quad \{\text{eqn:cost}\}$$

114 Choices of the times, t_i , t_f and the intervals of averaging, are at the disposal of the investi-
 115 gator and would normally reflect the purposes of the calculation. As a somewhat arbitrary
 116 reference for context here, December 2007 is chosen and the one-month average values are
 117 $\bar{J}_{MHT} = 1.1$ PW and $\bar{J}_{MVT} = 14.4$ Sv, the overbar denoting the average values (instead of a
 118 1-month average, a 1-year average could have been chosen; here we chose a 1-month average
 119 to exhibit more clearly the transient nature of the dual solution with respect to the objective
 120 function). The 1992 to 2007 mean values and standard deviations are $\langle J_{MHT} \rangle = 1.0 \pm 0.2$
 121 PW and $\langle J_{MVT} \rangle = 13.8 \pm 2.9$ Sv for meridional heat and volume transports, respectively,
 122 with standard deviations calculated from monthly mean ensemble members.

123 The latitude of 26°N is approximately that of the maximum in North Atlantic MHT and is
 124 the focus of the RAPID/MOCHA mooring array which was deployed in 2004 [*Cunningham*
 125 *et al.* 2007, *Kanzow et al.* 2007] and which has been used to document fluctuations in the J on
 126 a variety of time scales accessible with a few years of data. Simple theory and models suggest
 127 that J_{MHT} and J_{MVT} will vary due to a variety of causes ranging from local fluctuations
 128 e.g., in the wind field, to circulation variations that took place e.g., in the Southern Ocean
 129 decades earlier, and which are now being manifest at 26°N . Should local fluctuations clearly
 130 dominate the changes in the J on all time scales, the oceanographic observation problem is
 131 clearly far simpler than if one must cope with a global set of influences. One cannot afford,
 132 however, to simply assume that dominance.

133 2 The Method

134 The ocean model is that used in version 3 of the ECCO-GODAE state estimates [*Wunsch*
 135 *and Heimbach* 2007, *Wunsch et al.* 2009]. The model trajectory with respect to which
 136 sensitivities are calculated is one of the optimized ECCO-GODAE solutions for the period
 137 1992 and 2007. Configuration details are found in the Appendix. The dual (adjoint) model
 138 was generated via the automatic differentiation tool TAF [*Giering and Kaminski* 1998].
 139 To assess the robustness of the inferred sensitivities, results from a non-optimized solution
 140 are also presented (section 3.5). The adjoint model for the non-optimized integration was
 141 generated both with TAF and with the more recently developed automatic differentiation
 142 tool OpenAD [*Utke et al.* 2008] for the purposes of testing the dual models against each

143 other. The inferred sensitivities were found to be extremely similar. While a technical detail,
 144 the use of both TAF and OpenAD serves the purpose of demonstrating that MITgcm adjoint
 145 model generation can now be achieved with two independent AD tools.

146 Adjoint models are stable when integrated in the backward-in-time direction—corresponding
 147 to a determination of the propagation in space and time *from which* a disturbance at time
 148 t has emanated. Here the adjoint is integrated for 16 years backwards in time to January
 149 1992. Formally, it furnishes the full set of time-varying Lagrange multipliers—which are
 150 equivalent to the sensitivities at each timestep, t . That is, if the forward model state vector
 151 is $\mathbf{x}(t)$, then to each element of the state $x_i(t)$, access is available to any dual variable,
 152 denoted as

$$153 \quad \delta^* x_i(t) = \frac{\partial J}{\partial x_i(t)}. \quad (2) \quad \{\text{eqn:dual}\}$$

154 Snapshots every 15 days for various dual variables were saved for analysis. Here the focus
 155 is on elements of the oceanic state (temperature, salinity, pressure, and velocity). Equally
 156 important are sensitivities to the time-varying air-sea fluxes of momentum and buoyancy,
 157 but whose discussion we defer to a separate work in the interest of keeping the wealth of
 158 material manageable, and point to recent work in this regard by *Czeschel et al.* [2010].

159 As can be seen in eqn. (1) the objective functions differ in that J_{MHT} computes correlated
 160 effects between the temperature and velocity fields over the full water column, whereas
 161 J_{MVT} is a plain measure of velocity effects over only the upper ocean, albeit the temperature
 162 weighting also gives emphasis to the upper ocean. Their sensitivities are thus expected to
 163 differ, in particular where zonally dependent temperature variations are significant.

164 A necessary consideration is how to assess the importance of regional sensitivities against
 165 each other, and the relative importance of sensitivities to different variables. First, recall
 166 that the sensitivities are related to actual changes in the objective function via the Taylor
 167 series expansion of J in the vicinity of a point x_{i0} of the form

$$168 \quad J(x_i) = J(x_{i0}) + \left. \frac{\partial J}{\partial x_i} \right|_{x_0} \cdot (x_i - x_{i0}) + O(\|x_i - x_{i0}\|^2) \quad (3) \quad \{\text{eqn:taylor}\}$$

169 Eq. (3) suggests that a useful response estimate may be obtained from the gradients $\left. \frac{\partial J}{\partial x_i} \right|_{x_0}$
 170 by multiplying them with the actual anomalies, expected uncertainties in the observations,
 171 or the expected variability of x_i , i.e. $\sigma_i \sim (x_i - x_{i0})$.

172 The x_i are in practice components of different variables (such as temperature, salinity,
 173 surface forcing, model parameters) which we may distinguish via an index α , functions of
 174 time t and representative of three-dimensional vector fields; it is useful to acknowledge this
 175 specifically, by letting $i \rightarrow \alpha, i, j, k, t$. Then, using the three-dimensional a priori standard

176 deviation fields $\sigma_\alpha(i, j, k)$ for each variable $x_\alpha(t)$, and rescaling the δJ in terms of their
 177 mean values \bar{J} , the “normalized response fields” per unit depth are

$$\delta\tilde{J} = \frac{1}{\Delta z(k)} \frac{\delta J(x_\alpha(i, j, k, t))}{\bar{J}} = \frac{1}{\Delta z(k)} \frac{1}{\bar{J}} \left. \frac{\partial J}{\partial x_\alpha} \right|_{(i, j, k, t)} \delta x_\alpha(i, j, k), \quad \text{where } \delta x_\alpha = \sigma_\alpha$$
(4) {eqn:dualnormal}

178
 179 Eq. (4) accounts for sensitivities (and perturbations) that, when discretized, are a function
 180 of thicknesses $\Delta z(k)$ at level k . To be able to compare the impact of relevant temperature
 181 perturbations independent of the thickness of the vertical level at which they are calculated,
 182 the gradient, Eq. (2) is now normalized by the level thickness $\Delta z(k)$. Resulting units are
 183 thus in normalized responses per unit depth, i.e. [1/m]. Standard deviation fields used here
 184 for temperature and salinity are the ones presented in *Forget and Wunsch* [2007]. By way
 185 of example, Fig. 1 depicts $\sigma_T(i, j, k)$ for temperature ($\alpha = T$) at 222 m and 847 m depths.
 186 In the remainder of this paper, “sensitivities” always refer to the *normalized* ones.

187 Other choices of δx are conceivable, two of which we briefly mention, and each of which
 188 has its merit. One is the use of optimal perturbation patterns, i.e. patterns that are
 189 obtained from an optimization problem in which largest amplification of a specified norm
 190 (e.g. meridional volume transport) is sought. Thus, rather than expressing responses in
 191 terms of anomalies from “expected” uncertainties, anomalies are based on patterns that
 192 would lead to a maximum amplification. Such patterns, also called singular vectors, have
 193 recently been derived in an idealized GCM configuration by *Zanna et al.* [2010a,b]. The
 194 relationship between optimal patterns and expected uncertainty patterns remains to be
 195 explored in detail. Another approach would consist in calculating time-varying anomaly
 196 fields with respect to the mean over the model integration. MVT and MHT perturbations
 197 could then be reconstructed in terms of these anomaly fields. This approach was followed
 198 by *Czeschel et al.* [2010] who reconstruct AMOC changes from atmospheric perturbation
 199 anomalies in conjunction with adjoint forcing sensitivities.

200 3 Adjoint Pathways and Processes

201 The following provides a description of what could be termed a dual view of adjustment
 202 processes and time scales. Because of the correspondence of the adjoint model to the adjoint
 203 of a system of partial differential equations (e.g., Morse and Feshbach, 1953; Lanczos,
 204 1961), the dual model can be described in terms of, among other phenomena, *adjoint*
 205 Kelvin (coastal and equatorial) and Rossby waves.¹ These determine the relevant pathways
 206 and time scales by which information is transmitted in the forward model [*Galanti and*

¹The existence and use of “dual models” is commonplace in optimization theory of all kinds.

207 *Tziperman* 2003]. A full discussion here of adjoint physics is not possible, but note, for
 208 example, that the forward model tends to produce westward propagating Rossby waves
 209 from the eastern boundary, whereas in the dual model, it is the western boundary which
 210 generates eastward propagating analogues of Rossby wave physics (because information
 211 arrives at a point i, j, k at time t having travelled westward from further east, a backwards
 212 in time calculation of the region from which it arose involves propagation *eastward*).

213 Much of what follows is built on the descriptive result that the solution of adjoint wave
 214 problems are waves traveling in the opposite direction to their forward solution. To re-
 215 inforce this perspective, the terminology of *dual* Kelvin, *dual* Rossby, or *dual* continental
 216 shelf waves will be used. *Schröter and Wunsch* [1986] discuss the *dual* Gulf Stream, but
 217 the time-mean is not our present concern. Although adjoint models are linear ones, the
 218 reader will be aware that they are nonetheless full three-dimensional GCMs with all of the
 219 details and complexity of any other global scale fluid model, making the description of full
 220 solutions a considerable challenge.

221 3.1 Atlantic Signatures With Up to 4 Years Propagation Time

222 To begin the discussion, we first focus on the accessible time scale of about four years
 223 preceding December 2007. Figure 2 shows snapshots of MVT sensitivities to temperatures
 224 in the Atlantic from 0.1 years in the past back to 4 years earlier, at the depth of 222m.
 225 After four years (bottom right panel), the MVT sensitivity pattern is the result of the
 226 superposition of different processes and various “centers of action” seem to affect MVT. A
 227 brief description of the results in Figure 2 is now given, and Fig. 3 illustrates in a schematic
 228 way some of the main processes identified and described. Here, all times are given as years
 229 *before* December 2007:

Fig. 2

230 • *0.1 year*: The strongest (normalized, i.e. scaled by σ , see eqn. (4)) sensitivities are
 231 centered around the 26°N section and are an expression of the fast barotropic processes that
 232 are the only ones able to affect MVT on very short time scales. These sensitivities persist
 233 throughout the entire water column with essentially the same pattern (not shown). Positive
 234 sensitivities extending southward from 26°N are prominent along the eastern boundary
 235 (labeled [E1]) and enter the equatorial wave guide off the Gulf of Guinea (Africa, off Cote
 236 d’Ivoire). Negative sensitivities are apparent along the western boundary, extending from
 237 26°N to Flemish Cap (labeled [E2]). These patterns reflect the relatively fast connections
 238 along the boundaries provided by coastal Kelvin waves, which can exert control on MVT by
 239 changing pressure patterns near the eastern and western boundaries. Otherwise, sensitivities
 240 are also large near and along 26°N, reflecting Rossby wave processes that can affect the

Fig. 3

241 western boundary.

242 • *0.2 year*: The positive anomaly [E1] travels westward as an equatorial dual Kelvin wave
243 through the equatorial wave guide, reaches the coast of South America (off Brazil) from
244 where it sheds coastal dual Kelvin waves northward and southward into the corresponding
245 hemisphere. A first notable consequence is that the positive response anomaly now visible
246 off the South American coast (centered around French Guyana) is connected to 26°N , not
247 via a western basin direct connection (short circuit), but rather via an eastern basin origin,
248 having traveled from the eastern part of the basin (in adjoint sense) through the equatorial
249 wave guide.

250 A negative anomaly (labeled [E3]) is now visible off the African coast extending southward
251 from 26°N , having propagated eastward as expected from dual Rossby waves. The negative
252 anomaly along the western boundary [E2] reaches the Labrador Sea, remaining essentially
253 coastally trapped.

254 • *0.5 year*: The negative anomaly [E3] which had traveled east and southward from 15°N
255 along the African coast, enters the equatorial wave guide in the Gulf of Guinea. Positive
256 anomaly [E1] that has spread as a coastal dual Kelvin wave along South American coast
257 starts shedding dual Rossby waves into the interior. The mechanism for their reinforcement
258 is likely similar to the one described by *Galanti and Tziperman [2003]* in the Pacific as
259 delineating baroclinically unstable regions. Likewise, the negative anomaly along North
260 America [E2] radiates dual Rossby wave into the interior. Weak signals start to appear off
261 southern Greenland from [E2].

262 • *0.75 year (not shown)*: Positive anomalies propagate as dual Rossby waves [E1] in
263 a latitudinal band between 10 and 30°S are apparent, and having latitudinally dependent
264 propagation speeds. Negative anomaly [E3] has crossed the equator, now triggering a dual
265 coastal Kelvin wave along South America. The negative anomaly dual Rossby wave train
266 [E2] in the eastern North Atlantic between roughly 10 and 30°N is also clearly visible. A dual
267 coastal Kelvin wave (still linked to the original wave [E1]) reaches Cape Horn, surrounds it,
268 and continues along the Chilean coast (not shown), illustrating the very fast link between
269 the North Atlantic and the Southern Ocean through Kelvin wave dynamics. In a forward
270 sense, a perturbation entering the South Atlantic through the Drake Passage is propagated
271 equatorward as a coastal Kelvin wave, changes the side of the basin as an equatorial Kelvin
272 wave, and connects northward to 26°N as a coastal Kelvin wave along West Africa.

273 • *1 and 2 years*: All the above processes continue to evolve (backwards) in time. Equator-
274 ward propagating coastal Kelvin waves are unable to cross the equator, but instead change
275 sides of the basin in the equatorial wave guide before continuing poleward. The subsequent

276 propagation of information to the western side through the interior is quite slow. This
277 result confirms the idea of an equatorial buffer (e.g., *Johnson and Marshall* [2002, 2004]),
278 although it should be noted that, despite the delay, the influence of the southeastern part
279 of the Atlantic on these long time scales remains important. A signature of the β -effect in
280 an adjoint sense is clearly visible, especially south of the equator where the positive lobe
281 between 15°S and 30°S shows a southwest-to-northeast tilt. This result is consistent with
282 the basic properties of the corresponding *forward* Rossby waves whose phase speed increases
283 towards the equator (e.g., *Chelton and Schlax* [1996], *Killworth et al.* [1997]).

284 • *3 years (not shown)*: The positive dual Rossby wave-trains from [E1] have reached
285 the eastern part of the Atlantic basin, in the northern hemisphere bounded between 15°N
286 and 35°N off West Africa, in the southern hemisphere between 15°S and 35°S off Namibia.
287 Interestingly, there seems to be a northern barrier in the North Atlantic and a southern
288 barrier in the South Atlantic. The origin of the latter is probably the Antarctic Circumpolar
289 Current, whereas the origin of the former is not obvious. At least three possibilities exist:
290 (1) Slow westward propagation of Rossby waves is Doppler-shifted through superposition
291 with the mean flow associated with the subtropical gyre, the Gulf Stream and its North
292 Atlantic current extension. (2) The dual Rossby waves need land in the east from which
293 their forward counterparts are radiated. In the SH, the meridional extent is limited by the
294 southern tip of Africa, in the northern hemisphere by the northern limit of Africa and the
295 Strait of Gibraltar (*Fukumori et al.* [2006], based in adjoint calculations, have reported on
296 basin-wide sea-level fluctuations in the Mediterranean due to fast boundary Kelvin waves).
297 (3) The confinement may be associated with regions of baroclinic instabilities and where
298 sensitivities are amplified in the sense discussed by *Galanti and Tziperman* [2003].

299 Another noteworthy feature is that dual Rossby waves seem to be absorbed at the eastern
300 boundary—an analogue of dissipative westward intensification in the forward dynamics.
301 Some of it, however, likely arises from the generation of dual Kelvin waves at the coast.

302 • *4 years*: Apart from negative anomalies in the Labrador Sea and around Iceland, and
303 other signals near the western boundary north of 26°N , which might suggest involvement of
304 advective processes, most of the large sensitivities lie in the eastern part of the basins both
305 for the North and South Atlantic. These are associated primarily with the slow propaga-
306 tion of dual Rossby wave trains along the 26°N section, and in the South Atlantic as relics
307 from events [E1], [E3]. While sensitivities near 26°N might control the MVT by directly
308 communicating interior perturbations to the western boundary, the connection to the east-
309 ern South Atlantic occurs through several processes. Perturbations near the southern tip
310 of Africa (possibly triggered e.g., via Agulhas leakage) can lead to forward Rossby waves,
311 which are received off the coast of Brazil (after ~ 3 years), propagate towards the equator as

312 coastal Kelvin waves, enter the equatorial wave guide and are propagated eastward as equa-
 313 torial Kelvin waves, then northward along the West African coast, eventually connecting to
 314 26°N on the eastern boundary. Fig. 4

315 Some of the mechanisms described for the near-surface (222m) remain relevant near the base
 316 of the thermocline, e.g. at 847 m depth as depicted in Fig. 4: fast signal propagation through
 317 barotropic waves around 26°N, dual Kelvin waves, the equator serving both as barrier and
 318 wave guide, positive anomaly delivery off South America ([E1]), and fast negative anomaly
 319 propagation off North American coast ([E2]).

320 The South Atlantic dual Rossby wave signal is much weaker, presumably because 847m is
 321 below the depth of the strongest baroclinic instabilities. In the North Atlantic a strong
 322 negative response signal emerges beyond 0.5 years. The interpretation is that of an efficient
 323 connection between 26°N and mid-latitude dual Rossby waves through coastal dual Kelvin
 324 waves. From a forward perspective, it points to a negative influence of Rossby waves
 325 carrying positive temperature anomalies at mid-latitudes. Once these anomalies reach the
 326 western boundary, they are efficiently transmitted to 26°N where they effectively reduce
 327 the northward volume transport. At 30°S, eastward traveling dual Rossby waves which are
 328 prominent at 222 m depth, are still discernible at 847 m, but quite weak.

329 Maps similar to those depicted in Figure 2 and 4 can also be produced for any prognostic
 330 variable, all of which possess dual variables (i.e. time-dependent Lagrange multipliers). In
 331 particular, *salinity* instead of *temperature* response maps were analyzed, but are omitted
 332 here for the sake of space. They show strong similarity in patterns, and the reversed sign
 333 indicates the opposite (compensating) effect of salinity and temperature on density and a
 334 basic sensitivity of MVT to density perturbations. These effects are not further discussed
 335 here, but they are clearly important in any discussion of controls on the circulation. A
 336 detailed discussion of density effects in an idealized Atlantic configuration is provided by
 337 *Zanna et al.* [2010b] in the context of singular vector calculations. Response maps at depths
 338 will be further investigated in Section 3.7.

339 3.2 Amplitude-Weighted Time Scales

340 A crude but useful way to infer transit times of response signals is to consider the amplitude-
 341 weighted mean time, Fig. 5

$$342 \quad T_{tr}(i, j, k) = \frac{1}{N} \int_{t=0}^{16yr} t |\delta J(i, j, k, t)| dt \quad (5) \quad \{\text{eqn:weightedtim}$$

343 with normalizing factor $N(i, j, k) = \int_{t=0}^{16yr} \delta J(i, j, k, t) dt$. A spatio-temporally uniform δJ
344 would result in a uniform $T_{tr} = 8yr$. Maps of amplitude-weighted mean time at 222 m
345 and 1975 m depth (Fig. 5) clearly delineate fast time scales and pathways of sensitivities.

346 Prominent features are

- 347 (1) Localized sensitivities around 26°N (as expected);
- 348 (2) The Atlantic equatorial wave guide;
- 349 (3) The eastern seaboard of the Americas (North and South) as carrier of poleward-
350 traveling dual Kelvin waves;
- 351 (4) Subtropical Atlantic (5° to 35° latitude in both hemispheres) carrying dual Rossby
352 waves;
- 353 (5) Fast time scale motions leak through Drake Passage into the Pacific in the form of
354 (a) dual Kelvin waves along the Chilean coast, entering the Pacific equatorial wave guide,
355 changing sides of the basin as equatorial dual Kelvin waves, and shedding dual Rossby
356 waves in the western Pacific, and (b) westward dual propagation in the Southern Ocean (to
357 be discussed below), and likely the result of a Doppler-shifted westward moving forward
358 Rossby wave which is advected by a faster eastward-moving ACC;
- 359 (6) Reduced time scales in the Indian Ocean are a consequence of a connection through
360 fast dual Kelvin wave propagation along the South American coast, linked through the
361 tropical Pacific wave guide into the tropical Indian Ocean;
- 362 (7) Reduced time scale off the coast of Greenland.

363 Most noticeable in terms of the longest time scales are (i) the Nordic Seas (but whose
364 interpretation is cautioned in view of the lack of an Arctic ocean in the model), and to
365 some extent the central North Atlantic (surprising given the relative proximity to the 26°N
366 section and suggesting an important long term influence on MVT at 26°N); (ii) the eastern
367 subtropical Pacific; (iii) the Southern Ocean south of the ACC. As a note of caution, the
368 maps discussed here do not necessarily reflect *significant* regions of influence, because some
369 of the very short time scales of influence may be associated with very low amplitudes
370 of sensitivities (e.g. the tropical Pacific signal). Nevertheless, they do represent robust
371 coherent patterns with underlying dynamical origins.

372 3.3 Zonal and Meridional Sections Through Time

Fig. 6, 7

373 Further evidence for zonal propagation of sensitivities comes from the analysis of longitude
374 vs. time diagrams at a given latitude and depth. Figs. 6 and 7 depict such diagrams
375 for MVT and MHT sensitivities, respectively. As an example, consider in Fig. 6 the panel
376 representing MVT sensitivities at 27.5°N at 222 m depth (left column, 3rd row). A wave-like

377 dipole pattern hints at an eastward traveling dual Rossby wave which crosses the Atlantic
378 in roughly 7 to 10 years. Similar patterns are visible at 1975 m depth, both at 27.5°N and
379 at 41.5°N. The near-surface 41.5°N panel exhibits significant sensitivities in the western
380 part of the basin out to 15 years back in time, but which apparently do not cross the entire
381 basin in a similar fashion. A possible cause is the interaction of waves with a sheared flow
382 in parts of the basin, and which may alter the dual propagation speed.

383 Further north, the comparatively weak sensitivities at 57.5°N are perhaps surprising, given
384 the prominence in the literature attributed to this region in influencing the MVT. One
385 apparent result is that at no time do high-latitudes dominate the sensitivities (notice though
386 the limitation of absence of an Arctic ocean in the model).

387 In the southern hemisphere, the section at 28.5°S (bottom panel) reveals the dual Rossby
388 wave crossing the South Atlantic, taking about five years to do so, and providing a dynam-
389 ical link between the Agulhas leakage region and 26°N. The signal is prominent at 222m
390 depth, but essentially absent below the thermocline (1975m depth), suggesting a weakened
391 influence of the South Atlantic at depth both for MVT and for MHT sensitivities (bottom
392 panels of Figure 9).

393 Finally, the panel at 1°S clearly shows the equatorial wave guide as the fastest connector
394 between eastern and western Atlantic. Comparing Figs. 6 and 7 reveals similarities and
395 differences between the MVT and MHT response patterns. These will be discussed in more
396 detail in the context of latitude-time sections, but note, for example, large patterns of
397 opposite signs for 1°S and 27.5°N at 222 m depth, or differences in patterns at 27.5°N at
398 1975 m depth.

Fig. 8, 9

399 Normalized responses are plotted in Fig. 8 as Atlantic time-latitude diagrams along fixed
400 meridians (top panels: 45°W, bottom panel: 15°W). Also shown in Fig. 9 are panels repre-
401 senting the progression through time of the zonally integrated sensitivities at each latitude
402 at 222 m (top panels) and 1975 m depth. Both figures show MVT sensitivities in the left
403 column and MHT sensitivities in the right column. Note that while strong sensitivities
404 might be present at fixed meridians and at certain latitudes (consider, e.g. the prominent
405 positive MVT sensitivity at 35°N, 15°W, between roughly 4 to 10 years in the bottom left
406 panel of Fig. 8), the zonally integrated effect at this latitude is considerably weaker, if not
407 reversed (top left panel of Fig. 9).

408 3.4 Meridional Coherence

409 In the thermocline, an important (positive) contribution from southern latitudes up to about
410 10 years back in time is clearly visible. Also apparent is the negative influence from sub-polar
411 regions (poleward of 45°N). The “boomerang” shape reflects the reduction of speed of dual
412 Rossby waves with latitude, likely an effect of advection by the mean flow (Gulf Stream and
413 North Atlantic current). This meridional change in character of sensitivities, in particular
414 the increase in time scales of influence with latitude is consistent with findings by, e.g.,
415 *Bingham et al.* [2007]. Their study finds a lack of meridional coherence of the AMOC, with
416 a prominence of decadal variability north of roughly 40°N in contrast to higher-frequency
417 fluctuations to the south. Our findings support their caution in interpreting MOC variations
418 recorded at any one latitude. The mechanisms revealed here in terms of the time-evolving
419 dual fields may help to shed light on the causes of meridional sensitivity structure.

Fig. 10

420 A different way to assess the meridional coherence of the MVT is through a separate adjoint
421 calculation of MVT sensitivities evaluated in the subpolar gyre at 48°N, instead of 26°N.
422 A sample result of such a calculation is depicted in Fig. 10, showing response maps to
423 temperature perturbations at 222 m depth, which can be readily compared to corresponding
424 response maps shown in Fig. 2 for the 26°N adjoint calculation. The corresponding long-
425 term mean MVT at 48°N is $\langle J_{MVT} \rangle = 15.3 \pm 2.5$ Sv. The most striking differences are
426 the much reduced response amplitudes in the sub-tropical gyre for the 48°N case, and an
427 increased response north of Island. A time-lag of roughly half a year between the 26°N
428 and the 48°N calculation in tropical responses is also apparent. A robust feature in both
429 calculations is the response pattern in the southeast Atlantic 4 years back in time.

430 The example serves to underline previous findings of a lack of meridional coherency of the
431 MOC in the North Atlantic, a fact that needs to be taken into account when choosing
432 climate-relevant target norms for sensitivity calculations, and when inferring of regions of
433 dominant responses.

434 3.5 Meridional Volume Versus Heat Transport

435 Fig. 9 allows for a comparison of time-latitude responses for MVT and MHT. The response
436 fields calculated via Eq. (4) are normalized so as to provide a basis for comparison, both
437 among responses to different variables, as well as between the MHT and MVT responses.
438 Of particular interest is an assessment of the extent to which response patterns for MVT
439 correspond to those for MHT. In other words, we wish to know whether responses in MVT
440 to e.g., temperature perturbations, result in correlated responses to MHT changes. For the

441 sake of example, we focus on the zonal sum patterns (bottom panels) for MVT (left) vs.
 442 MHT (right).

Fig. 11

443 Because δJ_{MHT} and δJ_{MVT} have been normalized (both with respect to their respective
 444 means \bar{J} and with respect to the perturbation applied estimated through in-situ variabilities
 445 σ) so as to be of similar magnitudes for the same perturbation applied, see eqn. (4), we can
 446 obtain a first crude impression by simply subtracting these normalized fields and scaling
 447 the residual obtained against the range of the field, thus:

$$448 \quad R(lat, t) = \frac{1}{\gamma} (\delta J_{MHT} - \delta J_{MVT}) \quad (6)$$

449 with a range value of $\gamma = 5 \cdot 10^{-6}$. The result is plotted in Fig. 11 for 222 m (top) and
 450 1975 m depth (bottom). In the figure we have suppressed all signals for which the range of
 451 δJ_{MHT} itself is less than 20% of γ to focus on sizable signals only.

452 Small values of $R(lat, t)$ indicate latitudes (and times) where δJ_{MHT} and δJ_{MVT} act syn-
 453 chronously, i.e. increase in one variable corresponds to a (scaled) increase in the other. The
 454 most prominent such region is the North Atlantic, poleward of about 40°N out to 10 years,
 455 during which the responses have a sizable impact at 26°N.

456 In contrast, large (absolute) values in the figure correspond to latitudes (and times) for
 457 which the response of δJ_{MHT} is of opposite sign to that in δJ_{MVT} , or strong response in
 458 one quantity is not matched by a comparable response in the other, or the two lag each
 459 other. For example, temperature perturbations in the tropical Atlantic (15°N to 15°S)
 460 are persistently of opposite sign out to roughly 3 years, with δJ_{MHT} being positive and
 461 δJ_{MVT} negative (Fig. 9). In the latitudinal band between roughly 15°N and 40°N there
 462 is a very pronounced sign change in $R(lat, t)$. Interpretation in the context of monitoring,
 463 then suggests that observations of temperature anomalies at e.g., 26°N, would have quite
 464 different consequences for transport estimates at the same location if taken 2 years ahead
 465 versus those taken 4 years ahead.

466 3.6 Optimized versus Non-optimized Solution

467 The question of the importance of the basic state (the model trajectory) with respect
 468 to which the *tangent* linearization is performed deserves attention. In other words, which
 469 response patterns are robust and independent of the model trajectory, and which aspects are
 470 highly dependent upon it? This issue is addressed by revisiting the MHT responses (Fig. 7)
 471 plotted as a function of time vs. longitude at various latitudes and depth levels, but for a
 472 non-optimized solution. The dual solution of the non-optimized trajectories were calculated

473 somewhat differently from the optimized dual: the *Large et al.* [1994] KPP vertical mixing
474 parameterization scheme has been omitted from the forward (and dual) model so as to
475 permit an exact adjoint calculation (the adjoint of the full KPP scheme is unstable in parts);
476 in contrast, the Gent-McWilliams/Redi parameterization [*Gent and McWilliams* 1990, *Redi*
477 1982] has been retained both in the forward and in the dual (note that in the optimized
478 solution used here, both KPP and GM/Redi are turned off in the reverse integration, making
479 the dual model an approximate linearization); and the integration period was extended to
480 20 years, i.e. the dual was integrated from December 2007 back to January 1988. (The
481 constrained solution runs from 1992 forward—because that is when the database becomes
482 of useful size with the advent of satellite altimetry.) Admittedly, the model configurations
483 differ in a relatively large number of features, thus putting a severe test on the dual solution’s
484 robustness. Nevertheless, the differences chosen here are typical across different model
485 setups encountered, such that their comparison is warranted. In contrast to the optimized
486 solution, the dual model for the non-optimized run has been generated both with the AD
487 tool TAF [*Giering and Kaminski* 1998] as well as with the new open-source AD tool OpenAD
488 [*Utke et al.* 2008], and both models yield the same result.

Fig. 12

489 Figure 12 is a comparable plot to Fig. 7, but for the non-optimized model trajectory. Com-
490 paring the two figures, the normalized responses for the non-optimized trajectory show
491 smoother signal propagation compared to the optimized trajectory. Nevertheless, most
492 of the patterns can be readily identified in both solutions in terms of their broad struc-
493 tures, pointing to robust large scale processes underlying the propagation mechanisms. In
494 particular, all aspects discussed in section 3.3 remain valid (albeit with slightly different
495 amplitude) for the non-optimized solution. Additional aspects are perhaps somewhat easier
496 to discern owing to the smoothness of the signal. For example, at depth (right column) one
497 sees a pronounced increase and broadening of the tilt of negative sensitivities in going from
498 27.5°N to 41.5°N to 57.5°N, indicative of the β -effect. What appears to be noise in the left
499 panels (e.g. at 57.5°N) is in fact an expression of the influence of the seasonal cycle in the
500 near-surface (222 m depth) fields.

501 The noise in the near-surface panels (222 m, left column) can in part be explained by the
502 influence of the boundary layer scheme that is present in the optimized calculation, but not
503 in the non-optimized calculation (e.g., effect of wind-induced deepening of the boundary
504 layer). The second source of “noise”, in particular at depth (right column) might stem from
505 the influence of the observations to which the model was fit. The loss of smoothness may be
506 interpreted as an attempt of the optimization to fit noisy observations, but to some extent
507 it is also an expression of the eddy-rich context in which these observations were collected.
508 One interpretation is that the smooth signal (or sensitivity) propagation apparent in the

509 non-optimized solution is an “optimistic” limit (in the sense of how well dual signals may
510 be discerned and tracked) of actual signal propagation in the real system in which smooth
511 propagation will interact with the eddy field, and be obscured as a consequence.

512 3.7 Abyssal Processes and Signatures Beyond 10 Years

513 Further analyses have been performed for depth levels of 1975 m and 2950 m. In general,
514 normalized response signals (which are provided per unit depth) tend to diminish. By
515 way of example, we revisit Fig. 6 (optimized solution) now focusing on the right column
516 which depicts zonal sections vs. time along several latitudes in the Atlantic at 1975 m
517 depth (corresponding panels for the non-optimized solution which are less noisy are in
518 Fig. 12). It is apparent that the near-surface propagation in the South Atlantic is absent at
519 depth. In the northern hemisphere, the “tilt” of sensitivity bands can be attributed to wave
520 propagation, with an increase in tilt reflecting a decrease in propagation speed. This type of
521 analysis may give some hints on where deep observations may matter for decadal-scale signal
522 detection from long-term observations. For example, sensitivities of the 26°N transports
523 to perturbations near 26°N subside beyond roughly 5 years, but remain significant further
524 north out to 10 years and beyond. In the South Atlantic, no sizable sensitivities remain at
525 depth beyond roughly one year.

Fig. 13

526 Beyond 10 years backwards-in-time, sensitivities generally weaken but are more widespread.
527 Near the surface, the dominant areas of influence remain confined to the Atlantic. However,
528 below roughly 2000 m depth, a band of sensitivities throughout the Southern Ocean emerges
529 after 10 to 15 years (e.g., Fig. 13 showing maps at 1975 m and 2950 m depth, 15 years back
530 in time), whose magnitude are of comparable size to Atlantic sensitivities at the same depth
531 and time. The MVT and MHT response maps look similar (not shown), which confirms that
532 changes there are largely carried by the volume transport fluctuations. Several patterns in
533 the Southern Ocean stand out:

534 (1) A seemingly steady area (over the period 10 to 15 yr back in time, but shown here
535 for only year 15) of positive sensitivities south of the Agulhas current system (between
536 0°E and 45°E, at roughly 50°S). One can speculate that the recirculation in the Agulhas
537 current system would generate disturbances on various time scales. Water masses may be
538 temporarily enclosed within the recirculation, with different instances of “release” leading
539 to different time scales which link this area to 26°N (recirculation regions as “time scale
540 capacitors”).

541 (2) A negative pattern in the South Pacific which an animation reveals to consist of a
542 slowly westward-moving (backward-in-time) dipole of positive and negative sensitivities.

543 Its underlying dynamics are likely the result of a Doppler shift of a westward propagating
544 Rossby wave by the eastward flowing ACC (e.g., *Hughes* [1995], *Fu* [2004], *Tulloch et al.*
545 [2009]). The net dual propagation speed is the wave speed superimposed on the current
546 speed.

547 (3) Amplitudes are comparable to those in the Atlantic at similar depths, where a dominance
548 of high northern and southern latitudes is discernible. The positive pattern near 50°S around
549 the Prime Meridian is again attributed to the Agulhas current system. A strong positive
550 pattern in the central North Atlantic slowly moves eastward (backward in time, not shown).

Fig. 14

551 The time evolution along specific latitude bands, invoked above, can be summarized via
552 zonal sections as function of time. Fig. 14 shows such a section through the Antarctic
553 Circumpolar Current (ACC) at 58°S, depicting sensitivities at four different depth levels
554 (the less “noisy” non-optimized solution has been chosen to focus on the broad features). It
555 clearly reveals vertical shear in the ACC (different “tilt” of zonal propagation through time
556 as function of depth). To the extent that the average ocean depth is 4000 m, and only the
557 top 2000 m is currently subject to frequent in-situ measurements (Argo) the sensitivities
558 at depth, both in the Atlantic as well as in the Southern Ocean, appear to point to the
559 importance of obtaining abyssal measurements, if one is interested in capturing relevant
560 contributions to MHT variability on time scales beyond a decade.

561 3.8 Atmospheric Impacts

562 As mentioned in the introduction, the main purpose of this study is on the ocean’s dual
563 space for the purpose of identifying main oceanic pathways and time scales in the context of
564 observing system design. Given the un-coupled nature of our model (ocean-only) we are not
565 able to assess atmospheric pathways and teleconnections. Thus, tightly coupled phenomena,
566 such as the El Nino Southern Oscillation (ENSO) [e.g. *Cane* 2010] would only partly be
567 represented by the sensitivity pathways as computed here. Nevertheless, our system does
568 allow for propagation in the ocean interior of sensitivities to surface forcing perturbations.
569 This aspect has recently been studied by *Czeschel et al.* [2010] who computed multi-decadal
570 sensitivities of the MVT to surface buoyancy forcing in the subpolar gyre, and identified a
571 pronounced oscillatory sensitivity with a roughly 15 to 20 year period.

572 In keeping with our focus on the comparison between MVT and MHC sensitivities for our
573 16-year state estimate we show, by way of example, zonally integrated sensitivities of MVT
574 and MHT to zonal wind stress perturbations as a function of latitude and time (Fig. 15). The
575 basic structure is very similar to the one in Fig. 9 of near-surface sensitivities to temperature.
576 This re-inforces the notion of signal propagation of surface forcing perturbations through

577 Kelvin and Rossby waves. Here, as in section 3.3 we find the strongest differences between
578 MVT and MHT sensitivities in the tropics out to 3 years, and at northern mid-latitudes up
579 to a decade.

580 This is illustrated further by time series taken from Fig. 15 at four latitudes, and shown
581 in Fig. 16. At 26°N, following an initial fast coherent response (less than a year), a strong
582 positive anomaly is visible in MVT but not in MHT sensitivities at 1 to 4 year time scales.
583 What appears as an oscillation with a negative lobe from 4 to 8 years out in MVT responses
584 (Fig. 15a at 26°N) is not mimicked by MHT responses with a small steady positive sensitivity
585 out to 8 years (Fig. 15b). Strong differences are also apparent at 10°N on short time scales
586 (1 to 3 years). The pronounced negative–positive lobe apparent in MVT sensitivities is not
587 mirrored by MHT sensitivities. At 60°N, the situation is rather different, with MVT and
588 MHT sensitivities following each other closely. Both exhibit a positive sensitivity anomaly
589 which persists up to a decade. A low frequency behaviour is also apparent in the South
590 Atlantic. At 40°S MVT and MHT sensitivities show a coherent 8-year positive anomaly
591 followed by a negative lobe of similar temporal extent. Inspection of Fig. 15 suggests Rossby
592 wave dynamics as a cause.

593 We emphasize again that no assessment of atmospheric pathways is possible within the
594 given setup, but they are probably significant. The complex spatial sensitivity patterns
595 imply that similarly complex atmospheric forcing patterns may result in rather different
596 responses of the MVT and MHT. In particular, the topic of stochastic optimals in the
597 atmospheric forcing context is not touched upon here (but see, e.g., *Kleeman and Moore*
598 [1997] for a discussion in the context of ENSO predictability). Detailed knowledge of atmo-
599 spheric forcing is thus an important ingredient in any ocean observing system which aims at
600 quantifying origins and pathways of ocean circulation changes. However, it can be expected
601 that the oceanographic community can take advantage of the substantial effort already in
602 place for numerical weather prediction, and focus on the oceanographic challenge of filling
603 the vast gaps remaining in ocean observations.

604 4 Discussion

605 4.1 Implications for observing system design

606 No actual observing system has been designed in this study, yet the elements for such a
607 design study have been laid out, and some preliminary conclusions can be drawn.

608 First, it is evident that a rigorous design study is a complex, yet worthwhile undertaking.

609 Among the most pressing questions are the determination of a set of most relevant, or “most
610 important” (in some form to be agreed upon) metrics which serve as objective functions
611 for sensitivity calculations. An incomplete list among which to choose, are regional (or
612 near-coastal) property transports (zonal or meridional), sea surface temperatures, heat or
613 freshwater content, or sea level. An anticipated outcome, backed up by comparing MVT
614 and MHT, is that sensitivity patterns and time scales will depend on the metric chosen and
615 the region of interest.

616 A second complicating issue is the choice of regional foci. For example, while the altimetric
617 record suggests a global mean sea-level rise of 3 mm/year from 1993 to present, regional
618 expressions differ greatly, with a 1.5 cm/year rise in the western tropical Pacific accompanied
619 by a 2 mm/year drop in the eastern tropical Pacific, and an ambiguous picture along the
620 US eastern seaboard [*Nicholls and Cazenave* 2010].

621 Third, for a set of given objective functions, sensitivity pathways may be spatially or time-
622 lag correlated, given the basin-mode type structure of many of the patterns. This may
623 provide patterns of redundant information in the sensitivity structure (e.g. significant lag
624 correlations of sensitivity patterns) for different objective functions. In many cases the
625 boundaries serve as an efficient meridional communicator (along with the tropical wave
626 guide as zonal communicator) for dual Kelvin waves. For climate-relevant observations,
627 an important consideration will have to be to weigh response amplitudes against expected
628 eddy variability in order to maximize signal-to-noise ratios.

629 Fourth, the role of the forward state around which the linearized sensitivities were calculated
630 needs to be carefully assessed.

631 Fifth, the results will have to be considered in the light of technological capabilities and
632 costs. A particularly troubling element in this regard are the deep sensitivities in the South
633 Atlantic and their spreading into the Southern Ocean at long lead times (here considered
634 15 years, see Fig. 13). Apart from difficulties stemming from the remoteness of the region
635 (the Southern Ocean remains sparsely sampled even today), obtaining the relevant deep
636 observations would be technologically difficult and programmatically challenging because
637 of the long-term commitment required for their maintenance.

638 In the context of past observations, another consequence is that reconstructing heat and
639 volume transport variability on decadal time scales and beyond from past observations
640 may be limited by the sparse sampling of the Southern Ocean. Similarly troubling are the
641 complementarity of salinity vs. temperature sensitivities (their tendency to compensate for
642 density) in view of the much more limited number of salinity observations available in the
643 past, compared to those for temperature (XBTs).

region	LAT	LON	time	δJ @ 222m	δJ @ 1975m
NW sub-polar	45°N–60°N	75°W–15°W	1yr	-0.048 PW	-0.022 PW
			4yr	-0.032 PW	-0.029 PW
			7yr	-0.041 PW	-0.009 PW
NE sub-tropics	15°N–30°N	30°W–0°W	1yr	0.010 PW	$-4.3 \cdot 10^{-4}$ PW
			4yr	-0.028 PW	-0.006 PW
			7yr	0.025 PW	-0.0015 PW
Equator	5°S–5°N	45°W–0°W	1yr	0.030 PW	0.007 PW
			4yr	0.009 PW	0.002 PW
			7yr	$9.2 \cdot 10^{-4}$ PW	-0.001 PW
SE sub-tropics	40°S–25°S	0°E–15°E	1yr	$-9.6 \cdot 10^{-4}$ PW	$-1.9 \cdot 10^{-4}$ PW
			4yr	0.020 PW	0.002 PW
			7yr	0.024 PW	0.001 PW

Table 1: A list of anticipated changes in MHT inferred from adjoint sensitivities to temperature for several instances back in time (4th column) and perturbation regions. Perturbed MHT were calculated applying near surface (222m, next-to-last column) and deep (1975m, last column) temperature perturbations, integrating sensitivity fields over an area given by LAT (2nd column) and LON (3rd column), and applying a common thickness of $dz=500\text{m}$. Reference MHT is $\bar{J}_{MHT} = 1.1$ PW.

644 The richness of the time-evolving dual state space is evidently comparable to that of the
645 forward state. It implies that extensive analyses are required and care has to be taken in
646 interpreting the patterns inferred. Conclusions drawn depend on various “weights” (implicit
647 or explicit) and require close consultation between the modeling and the observational
648 community. Thus, what emerges may be considered as a long-term program for conducting
649 quantitative observing system design.

650 4.2 Preliminary conclusions

651 The major purpose here has been to demonstrate that the sensitivity of major elements of
652 the climate system to temporal and regional disturbances in the ocean state can be read-
653 ily determined using dual models, that the results are interesting and physically plausible.
654 Although a somewhat arbitrary subset of the enormous number of possibilities for observ-
655 ing climate-related shifts in the ocean has been selected, and no observational system has
656 actually be designed, some useful conclusions are possible:

657 (1) The dual state provides valuable information, complementary to the forward model
658 state, and whose detailed analysis is both rewarding and as challenging as the analysis of

659 the forward GCM. The complementarity is most visible in the role of Kelvin and Rossby
660 wave propagation in setting barotropic and baroclinic adjustment time scales, as discussed,
661 e.g., by *Johnson and Marshall* [2002, 2004].

662 (2) In the context of the observation and monitoring of key climate indices such as meridional
663 heat or volume transports at specific sections, significant sensitivities of similar magnitude
664 are not purely local, but extend throughout the Atlantic on time scales up to 10 years, with
665 signals emanating from increasingly remote places. For example, Fig. 2 indicates that at
666 four years back in time, several remote “centers-of-action” conspire to influence the MVT
667 at 26°N.

668 (3) Responses in seemingly similar climate indices such as those investigated here (J_{MHT}
669 vs. J_{MVT} , 26°N vs. 48°N) may differ substantially in (scaled) amplitude and sign and as
670 a function of time, making it difficult to infer responses of one quantity from those of the
671 other. One must carefully consider which indices are the most relevant in the context of
672 climate monitoring (or prediction). In particular, interchangeable use of MVT and MHT
673 variability obscures the underlying causal processes.

674 (4) Transient sensitivities are dual manifestations of dynamical processes underlying the
675 global oceanic teleconnections discussed in the context of climate variability (e.g., *Liu and*
676 *Alexander* [2007]). The schematic presented in Fig. 5 shows some time scales of what could
677 be termed dual teleconnections. Among the striking features are fast time scales connecting
678 26°N in the Atlantic (a) to the near surface Southern Ocean west of Cape Horn and the
679 western tropical Pacific (O(4) and O(6) years, respectively), and (b) to the (tropical) Indian
680 Ocean (O(7)) years. The latter has to come through the link of dual Kelvin waves along
681 the east and west coast of South America, the tropical Pacific, and leaking through the
682 Indonesian passages.

683 (5) Also noteworthy is that in none of the results presented, did the high northern latitudes
684 of the North Atlantic stand out as dominating regions of sensitivities (but notice the lack
685 of an Arctic ocean in the model). This result may appear surprising, given the prominent
686 role ascribed to these regions in the literature as apparent key regions influencing MVT and
687 MOC variability.

688 (6) A contribution to MVT variability discussed recently by *Biastoch et al.* [2008b] on
689 time scales of half a decade involves eddy shedding in the Agulhas retroflection region,
690 propagating westward in the South Atlantic toward the coast of Brazil, advecting northward
691 with the Brazil current and connecting with the Gulf Stream. Although our model does
692 not resolve such eddies, there is clear evidence for such a South Atlantic link (but here
693 represented by Rossby and Kelvin waves) within the thermocline in the results.

694 (7) A clear exposure of the Doppler effect in the Southern Ocean which the fast eastward-
695 flowing ACC exerts on westward-propagating Rossby waves (for zero mean flow) and which
696 leads to Doppler-shifted eastward Rossby wave propagation (e.g., *Hughes* [1995], *Fu* [2004],
697 *Tulloch et al.* [2009], but see also *Chelton et al.* [2007a] for caveats in the presence of eddies
698 and their eastward advection by the ACC).

699 Table 1 provides some numbers for hypothetical perturbations in various regions and at
700 different instances in time. The next-to-last column shows changes in MHT (in PW) for
701 perturbations applied near-surface (around 222m depth) over various geographical regions
702 (columns 1 to 3). The fourth column lists the prior uncertainty, σ , that sets the pertur-
703 bation amplitude chosen. Values of $\delta J = 0.04$ PW indicate a roughly 4% change in MHT
704 compared to the reference value of $\bar{J}_{MHT} = 1.1$ PW. Local and remote regions contribute
705 similar amounts to MHT variations. For example, changes in MHT due to temperature per-
706 turbations in the northwest sub-polar Atlantic seven years backward-in-time exceed those
707 due to temperature changes in the northeast sub-tropics one to four years earlier in time.
708 Furthermore, the latter are comparable to MHT changes arising from perturbations in the
709 southeast subtropical Atlantic 4 to 7 years back in time. Temperatures at depth (chosen
710 here as 1975m) lead, overall, to smaller MHT changes, but are of increasingly remote origin.

711 The sensitivity analyses presented here delineate a method to describe and quantify causal
712 connections (pathways, timescales, and response amplitudes) between climate diagnostics
713 (here Atlantic MVT and MHT), the large-scale circulation and the forcings. On time scales
714 of years to decades, a spatial pattern emerges which identifies various potential centers-of-
715 action that conspire in influencing variations in those climate diagnostics. Up to roughly
716 a decade wave-like adjustment processes dominate in amplitude. Beyond a decade, effects
717 of advection may become important. On shorter time scales advection may be relevant
718 in modulating wave propagation. The cautionary note by, e.g. *Bingham et al.* [2007] of
719 limited information content in MOC recordings at any one latitude for determining the
720 overall North Atlantic circulation is supported by our transient sensitivity results.

721 A general limitation of this study is that the model resolution does not admit or resolve
722 mesoscale eddies. Whereas many of the identified signals are here interpreted in terms
723 of wave dynamics, high-resolution simulations suggest a significant role for eddies, e.g. in
724 exchange processes between the sub-polar and sub-tropical North Atlantic, the link between
725 the Indian Ocean and the North Atlantic via the Agulhas retroflection, variability in the
726 Brazil current, or the dynamics of the ACC. Future work should assess to which extent
727 inferred sensitivities carry over to eddy-admitting or fully resolving resolutions. Such work
728 will have to address the difficult question of distinguishing between (nonlinear) eddy-induced
729 effects, and those carried by (linear) Rossby wave propagation, both of which travel at

730 roughly the same speed [*Chelton et al.* 2007a, *Tulloch et al.* 2009]. Similarly, the role of
731 sharply defined continental boundary regions in supporting boundary wave propagation may
732 be underestimated in coarse-resolution models, as pointed out by *Greatbatch and Peterson*
733 [1996]. While our study shows the crucial link that these regions provide in terms of
734 “dynamic” teleconnections, an improved representation of the coastal and shelf wave guide
735 is clearly warranted.

736 To the extent that pathways are robust, and sensitivity (or response) amplitudes broadly
737 reasonable, the sensitivity maps may provide clues as to which regions are of heightened im-
738 portance for taking relevant observations. No model is completely realistic and the present
739 one is no exception. Nonetheless, many of the dominant sensitivities are robust because
740 they are dependent upon physically plausible ocean dynamics.

741 This analysis can be extended in numerous ways: to longer times; with the use of higher
742 resolution models; to explore sensitivities to meteorological forcing of the present and past;
743 to the use of different target functions; to model elements themselves (mixing coefficients,
744 water depths, etc.), and in particular to fuller exploration of the dynamics of the dual
745 system. On very long time scales, such work has already been performed with the analysis
746 of “equilibrium sensitivities” [*Bugnion et al.* 2006a,b].

747 Very recently, *Czeschel et al.* [2010] have investigated multi-decadal sensitivities to surface
748 forcing in a regional Atlantic configuration of the MITgcm at comparable resolution. Be-
749 cause meteorological observations are already near-global in scope, and likely to continue to
750 be so, sensitivity to atmospheric forcing is somewhat less urgent in the experimental design
751 context than are the more regional oceanographic observing systems. In a similar spirit,
752 *Heimbach et al.* [2010a] have also demonstrated the power of the dual space approach to
753 infer sensitivities of sea ice export through the Canadian Arctic Archipelago on inter-annual
754 time scales using a coupled ocean/sea ice adjoint model.

755 As for the dual system, singular vectors which shed light on regions and mechanisms of
756 non-normal transient amplification of the chosen diagnostic (formulated as a norm kernel)
757 hold the prospect of sharpening some of the analyses presented here [*Farrell* 1988, *Trefethen*
758 *et al.* 1993]. While patterns are likely similar to adjoint sensitivities, perturbation patterns
759 that are projected onto the adjoint fields are those which optimize the norm kernel over a
760 certain time, rather than those of estimated variability as chosen here. Perhaps a clearer
761 decomposition is obtained in terms of such optimal perturbation patterns, and work in
762 this regard has been undertaken in the context of the MITgcm by *Zanna et al.* [2010a,b,c].
763 These point to regions of highest uncertainties with regard to observations of the target
764 diagnostic. An important direction of research will be the extension of this work to realistic

765 configurations. Similar methods have been successfully applied to targeted observations
766 in numerical weather prediction [*Buizza and Palmer 1995, Gelaro et al. 1999*] and in the
767 context of ENSO dynamics and predictability [*Penland and Sardeshmukh 1995, Moore and*
768 *Kleeman 1997a*]. Approaches to approximate full singular vector calculations through the
769 use of eigenmodes of the linearized model operator have also been pursued in the context
770 of realistic GCM configurations [*Sevellec et al. 2008*].

771 The issue of the climate diagnostic elements is perhaps the most difficult one. Here two
772 indices (MHT, MVT) were adopted, and, as expected, are closely related. Nonetheless they
773 exhibit markedly different response patterns, especially in the vicinity of the correspondingly
774 arbitrary latitude used (26°N). Other diagnostics, such as upper ocean heat content, Drake
775 Passage transport, regional sea level, etc. need to be explored in similar fashion if they are
776 regarded as candidates for dominant elements of climate change.

777 *Acknowledgements.* We are grateful for useful comments from Martin Losch, and from
778 two anonymous reviewers. Supported in part through the “Estimating the Circulation and
779 Climate of the Ocean” (ECCO) and the “Atlantic MOC Observing System Studies Using
780 Adjoint Models” projects of National Oceanographic Partnership Program (NOPP) with
781 funding from NASA, and the NSF Collaboration in Mathematics and Geoscience (CMG)
782 project “Uncertainty Quantification in Geophysical State Estimation”. Computing support
783 came through facilities at the NASA Advanced Supercomputing (NAS) division and the
784 NCAR Scientific Computing Division (SCD).

785 Appendix: Model configuration

786 The calculations were performed with the MIT general circulation model (MITgcm) [*Mar-*
787 *shall et al. 1997a,b, Adcroft et al. 2002*] in the ECCO-GODAE version 3 configuration [*Wun-*
788 *sch et al. 2007, Wunsch and Heimbach 2009*]. It is characterized by a quasi-global domain
789 covering 80°N to 80°S at a $1^\circ \times 1^\circ$ horizontal resolution with 23 unevenly spaced height lev-
790 els. Vertical mixing is parameterized using the KPP scheme of *Large et al. [1994]*, isopycnal
791 diffusion and eddy transport are parameterized using the Gent-McWilliams/Redi schemes
792 [*Gent and McWilliams 1990, Redi 1982*]. The surface forcing is achieved with the *Large and*
793 *Yeager [2004]* bulk formulae which convert surface atmospheric state variables into air-sea
794 fluxes. A dynamic/thermodynamic sea ice model computes sea ice concentration, snow and
795 ice thickness, ice velocities, and modifies air-sea fluxes over ice-covered regions [*Losch et al.*
796 *2010*]. The model is integrated from January 1992 to December 2007 using adjusted initial
797 conditions and surface atmospheric state variables. These adjustments are the result of a
798 least-squares fit of the model to a variety of observations using the adjoint or Lagrange
799 multiplier method (for a list of observations used, see *Wunsch et al. [2009]*). The surface
800 boundary conditions consist of 6-hourly atmospheric state variables from the NCEP/NCAR
801 reanalysis [*Kalnay and 21 others 1996*] with superimposed daily adjustments of surface air
802 temperature, specific humidity, precipitation, downwelling shortwave radiation, and wind
803 speed vector.

804 The adjoint model required both for the gradient-based optimization as well as for the
805 sensitivity calculations was generated via automatic differentiation (AD, see, e.g., *Marotzke*
806 *et al. [1999], Heimbach et al. [2005], Griewank and Walther [2008]*). Sensitivity calculations
807 using the optimized solution are based on the adjoint model generated with the commercial
808 AD tool TAF [*Giering et al. 2005*]. For the non-optimized solution we generated the adjoint
809 both via TAF as well as the open-source tool OpenAD [*Utke et al. 2008*]. Both AD-generated
810 models show essentially the same results (as part of the routine test suite of the MITgcm,
811 adjoint models are now being generated on a nightly basis both with TAF and OpenAD to
812 ascertain that their results agree).

813 In addition to assessing the impact of the reference trajectory itself (optimized vs non-
814 optimized) we also assessed the omission of some of the physics in the adjoint model. The
815 adjoint of the optimized solution is approximate in the sense that sensitivities related to
816 the parameterization schemes are omitted. For the non-optimized sensitivity calculation
817 we omitted the KPP scheme in both the forward and adjoint calculation, but kept the
818 GM/Redi scheme active both in the forward as well as the adjoint simulation, i.e. we ran
819 an exact adjoint model.

820 References

- 821 Adcroft, A., J.-M. Campin, P. Heimbach, C. Hill and J. Marshall [2002], MITgcm Release1
822 Manual, (online documentation) , MIT / EAPS, Cambridge, MA 02139, USA.
- 823 Biastoch, A, C.W. Böning and J.R.E. Lutjeharms [2008b], ‘Agulhas leakage dynamics
824 affects decadal variability in Atlantic overturning circulation’, *Nature* **456**, 489–492.
825 doi:10.1038/nature07426
- 826 Bingham, R.J., C.W. Hughes, V. Roussenov and R.G. Williams [2007], ‘Meridional co-
827 herence of the North Atlantic meridional overturning circulation’, *Geophys. Res. Lett.*
828 **34**, L23606.
- 829 Bugnion, V., C. Hill and P. Stone [2006a], ‘An Adjoint Analysis of the Meridional Over-
830 turning Circulation in an Ocean Model’, *J. Clim.* **19(15)**, 3732–3750.
- 831 Bugnion, V., C. Hill and P. Stone [2006b], ‘An Adjoint Analysis of the Meridional Over-
832 turning Circulation in a Hybrid Coupled Model’, *J. Clim.* **19(15)**, 3751–3767.
- 833 Buizza, R. and T.N. Palmer [1995], ‘The singular-vector structure of the atmospheric global
834 circulation’, *J. Atmos. Sci.* **52**, 1434–1456.
- 835 Cane, M.A. [2010], *The El Niño-Southern Oscillation Phenomenon*, Cambridge University
836 Press, London.
- 837 Cessi, P., K. Bryan and R. Zhang [2004], ‘Global seiching of thermocline waters between
838 the Atlantic and the Indian-Pacific ocean basins’, *Geophys. Res. Lett.* **31**, L04302.
- 839 Cessi, P. and P. Otheguy [2003], ‘Oceanic teleconnections: remote response to decadal
840 wind forcing’, *J. Phys. Oceanogr.* **33**, 1604–1617.
- 841 Chelton, D., M.G. Schlax, R.M. Samelson and R.A. De Szoeke [2007a], ‘Global observations
842 of large oceanic eddies’, *Geophys. Res. Lett.* **34**, L15606. doi:10.1029/2007GL030812
- 843 Chelton, D.B. and M.G. Schlax [1996], ‘Global observations of oceanic Rossby waves’, *Sci-*
844 *ence* **272**, 234–238.
- 845 Cunningham, S. A., T. Kanzow, D. Rayner, M. O. Baringer, W. E. Johns, J. Marotzke,
846 H. R. Longworth, E. M. Grant, J. J.-M. Hirschi, L. M. Beal, C. S. Meinen and H. L.
847 Bryden [2007], ‘Temporal variability of the Atlantic meridional overturning circulation
848 at 26.5 degrees N’, *Science* **317**, 935–938. doi:10.1126/science.1141304

849 Czeschel, L., D.P. Marshall and H.L. Johnson [2010], ‘Oscillatory sensitivity of
850 Atlantic overturning to high-latitude forcing’, *Geophys. Res. Lett.* **37**, L10601.
851 doi:10.1029/2010GL043177

852 Farrell, B.F. [1988], ‘Optimal excitation of neutral Rossby waves’, *J. Atmos. Sci.* **45**, 163–
853 172.

854 Forget, G. and C. Wunsch [2007], ‘Global hydrographic variability and the data weights in
855 oceanic state estimates’, *J. Phys. Oceanogr.* **37(8)**, 1997–2008. doi:10.1175/JP03072.1

856 Fu, Lee-Lueng [2004], ‘Latitudinal and frequency characteristics of the westward propaga-
857 tion of large-scale oceanic variability’, *J. Phys. Oceanogr.* **34**, 1907–1921.

858 Fukumori, I., D. Menemenlis and T. Lee [2006], ‘A near-uniform basin-wide sea level fluc-
859 tuation of the Mediterranean Sea’, *J. Phys. Oceanogr.* **37**, 338–358.

860 Galanti, E. and E. Tziperman [2003], ‘A midlatitude–ENSO teleconnection mechanism via
861 baroclinically unstable long Rossby waves’, *J. Phys. Oceanogr.* **33**, 1877–1887.

862 Gelaro, R., R.H. Langland, G.D. Rohali and T.E. Rosmond [1999], ‘An assessment
863 of the singular-vector approach to targeted observations using the FASTEX dataset’,
864 *Q. J. R. Meteorol. Soc.* **125**, 3299–3327.

865 Gent, P.R. and J.C. McWilliams [1990], ‘Isopycnal mixing in ocean circulation models’,
866 *J. Phys. Oceanogr.* **20**, 150–155.

867 Giering, R. and T. Kaminski [1998], ‘Recipes for adjoint code construction’, *ACM Trans-*
868 *actions on Mathematical Software* **24**, 437–474.

869 Giering, R., T. Kaminski and T. Slawig [2005], ‘Generating Efficient Derivative Code with
870 TAF: Adjoint and Tangent Linear Euler Flow Around an Airfoil’, *Future Generation*
871 *Computer Systems* **21(8)**, 1345–1355.

872 Greatbatch, R.J. and K.A. Peterson [1996], ‘Interdecadal variability and oceanic thermo-
873 haline adjustment’, *J. Geophys. Res.* **101(C9)**, 20,467–20,482.

874 Griewank, A. and A. Walther [2008], *Evaluating Derivatives. Principles and Techniques*
875 *of Algorithmic Differentiation*, Vol. 19 of *Frontiers in Applied Mathematics*, 2nd edn.,
876 SIAM, Philadelphia, 442 pp.

877 Haine, T.W.N., H. Zhang, D.W. Waugh and M. Holzer [2008], ‘On transit-
878 time distributions in unsteady circulation models’, *Ocean Modelling* **21**, 35–45.
879 doi:10.1016/j.ocemod.2007.11.004

- 880 Haine, T.W.N. and T.M. Hall [2002], ‘A generalized transport theory: water-mass compo-
881 sition and age’, *J. Phys. Oceanogr.* **32**, 1932–1946.
- 882 Heimbach, P. [2008], ‘The MITgcm/ECCO adjoint modelling infrastructure’, *CLIVAR Ex-
883 changes* **44 (Volume 13, No. 1)**, 13–17.
- 884 Heimbach, P., C. Hill and R. Giering [2005], ‘An efficient exact adjoint of the parallel MIT
885 general circulation model, generated via automatic differentiation’, *Future Generation
886 Computer Systems* **21(8)**, 1356–1371. doi:10.1016/j.future.2004.11.010
- 887 Heimbach, P., D. Menemenlis, M. Losch, J.M. Campin and C. Hill [2010a], ‘On the for-
888 mulation of sea-ice models. Part 2: Lessons from multi-year adjoint sea-ice export sen-
889 sitivities through the Canadian Arctic Archipelago’, *Ocean Modelling* **33(1-2)**, 145–158.
890 doi:10.1016/j.ocemod.2010.02.002
- 891 Holzer, M. and T.M. Hall [2000], ‘Transit-time and tracer-age distributions in geophysical
892 flows’, *J. Atmos. Sci.* **57**, 3539–3558.
- 893 Hughes, C.W. [1995], ‘Rossby waves in the Southern Ocean: A comparison of
894 TOPEX/Poseidon altimetry with model predictions’, *J. Geophys. Res.* **100**, 15 933–15
895 950.
- 896 Johnson, H.L. and D.P. Marshall [2002], ‘A theory for the surface Atlantic response to
897 thermohaline variability’, *J. Phys. Oceanogr.* **32**, 1121–1132.
- 898 Johnson, H.L. and D.P. Marshall [2004], ‘Global teleconnections of meridional overturning
899 circulation anomalies’, *J. Phys. Oceanogr.* **34**, 1702–1722.
- 900 Kalnay, E. and 21 others [1996], ‘The NCEP/NCAR 40-Year Reanalysis Project’,
901 *Bull. Am. Met. Soc.* **77(3)**, 437–471.
- 902 Kanzow, T., S. A. Cunningham, D. Rayner, J. J.-M. Hirschi, W. E. Johns, M. O. Baringer,
903 H. L. Bryden, L. M. Beal, C. S. Meinen and J. Marotzke [2007], ‘Observed Flow Com-
904 pensation Associated with the MOC at 26.5N in the Atlantic’, *Science* **317**, 938–941.
905 doi:10.1126/science.1141304
- 906 Khatiwala, S. [2007], ‘A Computational Framework for Simulation of Biogeochemical Trac-
907 ers in the Ocean.’, *Glob. Biogeochem. Cycles* **21**, GB3001. doi:10.1029/2007GB002923
- 908 Killworth, P.D., D.B. Chelton and R.A. De Szoeke [1997], ‘The speed of observed and
909 theoretical long extratropical planetary waves’, *J. Phys. Oceanogr.* **27**, 1946–1966.
- 910 Kleeman, R. and A.M. Moore [1997], ‘A theory for the limitation of ENSO predictability
911 due to stochastic atmospheric transients’, *J. Atmos. Sci.* **54**, 753–767.

- 912 Köhl, A. [2005], ‘Anomalies of Meridional Overturning: Mechanisms in the North Atlantic’,
913 *J. Phys. Oceanogr.* **35**(8), 1455–1472. doi:10.1175/JP02767.1
- 914 Large, W.G., J.C. McWilliams and S.C. Doney [1994], ‘Oceanic vertical mixing: A review
915 and a model with nonlocal boundary layer parameterization’, *Rev. Geophys.* **32**, 363–403.
- 916 Large, W.G. and S.G. Yeager [2004], Diurnal to decadal global forcing for ocean and sea-
917 ice models: the data sets and flux climatologies, Technical Note NCAR/TN-460+STR,
918 NCAR, Boulder, CO.
- 919 Liu, Z. and M. Alexander [2007], ‘Atmospheric bridge, oceanic tunnel, and global climatic
920 teleconnections’, *Rev. Geophys.* **45**, RG2005.
- 921 Losch, M., D. Menemenlis, J.M. Campin, P. Heimbach and C. Hill [2010], ‘A
922 dynamic-thermodynamic sea ice model for ocean climate modeling on an Arakawa
923 C-grid: Part 1: Forward model sensitivities.’, *Ocean Modelling* **33**(1-2), 129–144.
924 doi:10.1016/j.ocemod.2009.12.008
- 925 Marotzke, J., R. Giering, K.Q. Zhang, D. Stammer, C. Hill and T. Lee [1999], ‘Construction
926 of the adjoint MIT ocean general circulation model and application to Atlantic heat
927 transport variability’, *J. Geophys. Res.* **104**, C12, 29,529–29,547.
- 928 Marshall, J., A. Adcroft, C. Hill, L. Perelman and C. Heisey [1997b], ‘A finite-volume, in-
929 compressible Navier Stokes model for studies of the ocean on parallel computers’, *J. Geo-
930 phys. Res.* **102**, C3, 5,753–5,766.
- 931 Marshall, J., C. Hill, L. Perelman and A. Adcroft [1997a], ‘Hydrostatic, quasi-hydrostatic
932 and nonhydrostatic ocean modeling’, *J. Geophys. Res.* **102**, C3, 5,733–5,752.
- 933 Moore, A.M. and R. Kleeman [1997a], ‘The singular vectors of a coupled ocean-atmosphere
934 model of ENSO. I: Thermodynamics, energetics and error growth’, *Q. J. R. Meteorol. Soc.*
935 **123**, 953–981.
- 936 Nicholls, R.J. and A. Cazenave [2010], ‘Sea-level rise and its impact on coastal zones’,
937 *Science* **328**, 1517–1520. doi:10.1126/science.1185782
- 938 Penland, C. and P.D. Sardeshmukh [1995], ‘The optimal growth of tropical sea surface
939 temperature anomalies’, *J. Clim.* **8**(8), 1999–2024.
- 940 Primeau, F. and E. Deleersnijder [2009], ‘On the time to tracer equilibrium in the global
941 ocean’, *Ocean Sci.* **5**, 13–28.
- 942 Redi, M.H. [1982], ‘Oceanic isopycnal mixing by coordinate rotation’, *J. Phys. Oceanogr.*
943 **12**, 1154–1158.

- 944 Schröter, J. and C. Wunsch [1986], ‘Solution of nonlinear finite difference ocean mod-
945 els by optimization methods with sensitivity and observational strategy analysis’,
946 *J. Phys. Oceanogr.* **16**, 1855–1874.
- 947 Sevellec, F., T. Huck, M.B. Jelloul, N. Grima, J. Viardard and A. Weaver [2008], ‘Optimal
948 surface salinity perturbations of the meridional overturning and heat transport in a global
949 ocean general circulation model’, *J. Phys. Oceanogr.* **38**, 2739–2754.
- 950 Stammer, D. [2008], ‘Response of the global ocean to Greenland and Antarctic ice melting’,
951 *J. Geophys. Res.* **113**, C06022.
- 952 Trefethen, L.N., A.E. Trefethen, S.C. Reddy and T.A. Driscoll [1993], ‘Hydrodynamic sta-
953 bility without eigenvalues’, *Science* **261**, 578–584. doi:10.1126/science.261.5121.578
- 954 Tulloch, R., J. Marshall and K.S. Smith [2009], ‘Interpretation of the propagation of surface
955 altimetric observations in terms of planetary waves and geostrophic turbulence’, *J. Geo-
956 phys. Res.* **114**, C02005. doi:10.1029/2008JC005055
- 957 Utke, J., U. Naumann, M. Fagan, N. Tallent, M. Strout, P. Heimbach, C. Hill, D. Ozyurt and
958 C. Wunsch [2008], ‘OpenAD/F: A modular open source tool for automatic differentiation
959 of Fortran codes’, *ACM Transactions on Mathematical Software* **34(4)**, .
- 960 Veronis, G. and H. Stommel [1956], ‘The action of variable wind stresses on a stratified
961 ocean’, *J. Marine Res.* **15**, 43–75.
- 962 Wunsch, C. [2006a], *Discrete Inverse and State Estimation Problems : With Geophysical
963 Fluid Applications*, Cambridge University Press, Cambridge (UK), 400 pp.
- 964 Wunsch, C. and P. Heimbach [2007], ‘Practical global oceanic state estimation’, *Physica D*
965 **230(1-2)**, 197–208.
- 966 Wunsch, C. and P. Heimbach [2008], ‘How long to oceanic tracer and proxy equilibrium?’,
967 *Quat. Sci. Rev.* **28**, 637–651.
- 968 Wunsch, C. and P. Heimbach [2009], ‘The globally integrated ocean circulation (MOC),
969 1992-2006: seasonal and decadal variability’, *J. Phys. Oceanogr.* **39(2)**, 351–368.
- 970 Wunsch, C., P. Heimbach, R.M. Ponte and I. Fukumori [2009], ‘The Global General Circu-
971 lation of the Oceans Estimated by the ECCO-Consortium’, *Oceanography* **22(2)**, 88–103.
- 972 Wunsch, C., R.M. Ponte and P. Heimbach [2007], ‘Decadal trends in sea level patterns:1993-
973 2004’, *J. Clim.* **20(24)**, 5889–5911.

- 974 Zanna, L., P. Heimbach, A.M. Moore and E. Tziperman [2010a], ‘Optimal
975 growth of tropical Atlantic SST anomalies’, *J. Phys. Oceanogr.* **40(5)**, 983–1003.
976 doi:10.1175/2009JP04196.1
- 977 Zanna, L., P. Heimbach, A.M. Moore and E. Tziperman [2010b], ‘Optimal excitation of
978 interannual Atlantic meridional overturning circulation variability’, *J. Clim.* **in press.**, .
979 doi:10.1175/2010JCLI3610.1
- 980 Zanna, L., P. Heimbach, A.M. Moore and E. Tziperman [2010c], ‘Analysis of the pre-
981 dictability and variability of the Atlantic ocean in response to optimal surface excitation’,
982 *Quart. J. Roy. Met. Soc.* **submitted**, .

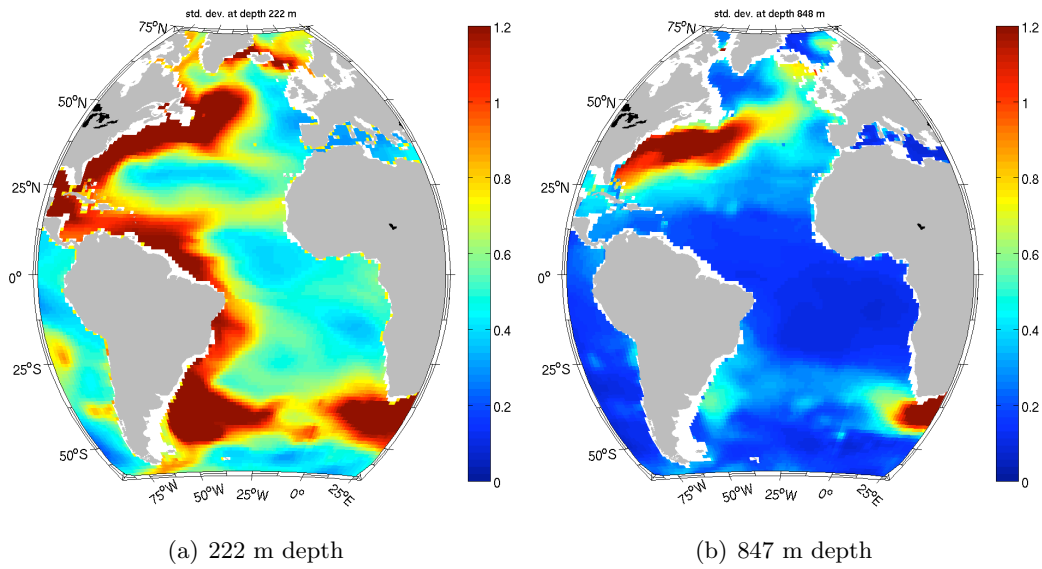


Figure 1: Maps of uncertainty estimates of in-situ observations for temperature in $^{\circ}\text{C}$ (but dominated by representation errors due to eddy variability) at different depth levels, based on *Forget and Wunsch* [2007], and used here to produce perturbation response estimates following eqn. (4). `fig:stddev-maps`

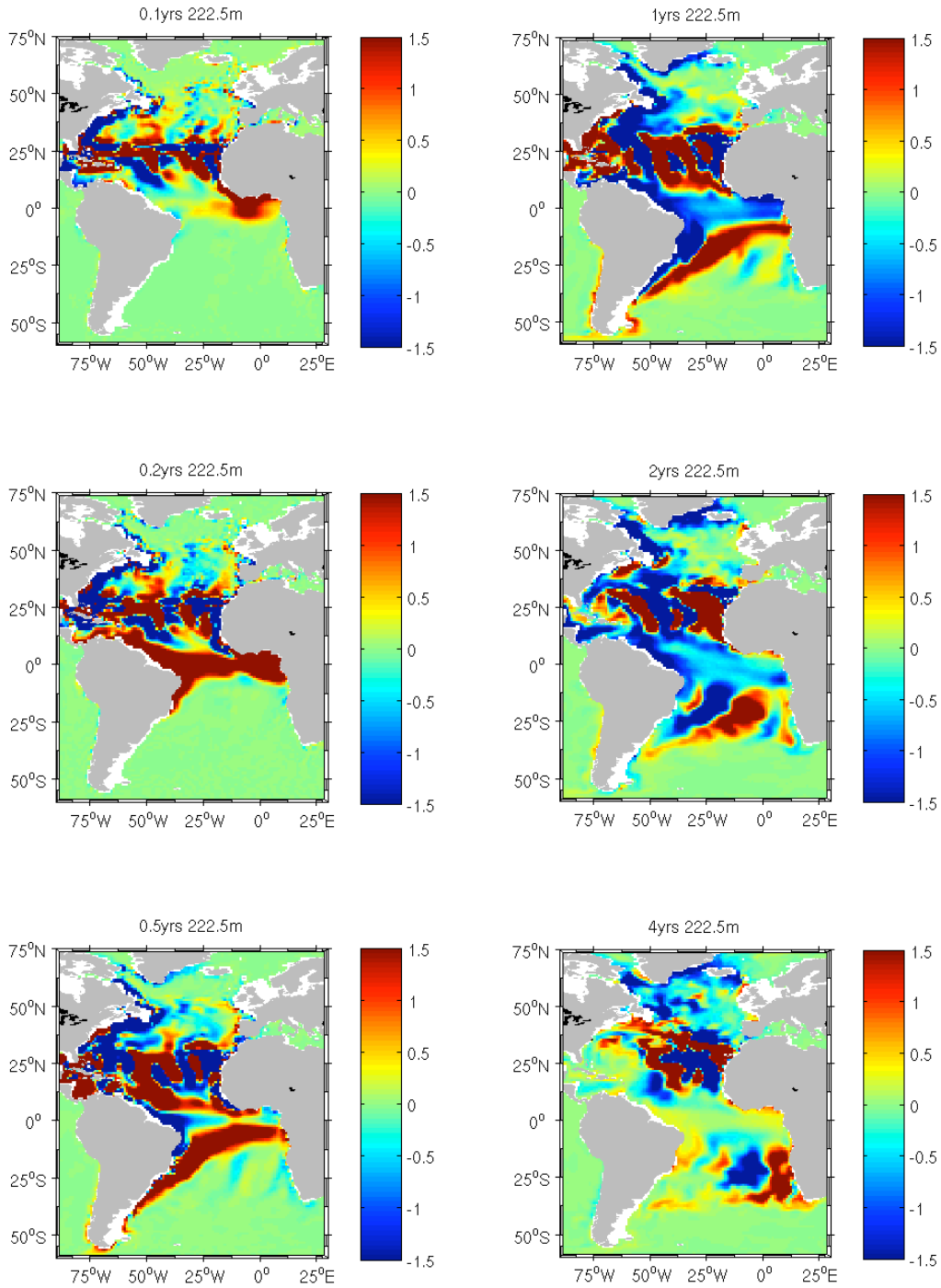


Figure 2: Maps of normalized response fields of meridional volume transport, δJ_{MVT} , to temperature changes in the Atlantic at 222 m depth, calculated with the adjoint and using eqn. (4). From top to bottom-left to top-to-bottom right they represent snapshots 0.1, 0.2, 0.5, 1, 2, and 4 years back in time. At each gridpoint the dual has been multiplied by the prior uncertainty estimate σ estimated by *Forget and Wunsch* [2007] and normalized by the cell thickness dz and by the value of J itself. Units are thus in $[1/m]$, but rescaled by a factor of 10^7 for convenience. **fig:35p-atl-0to4-k9**

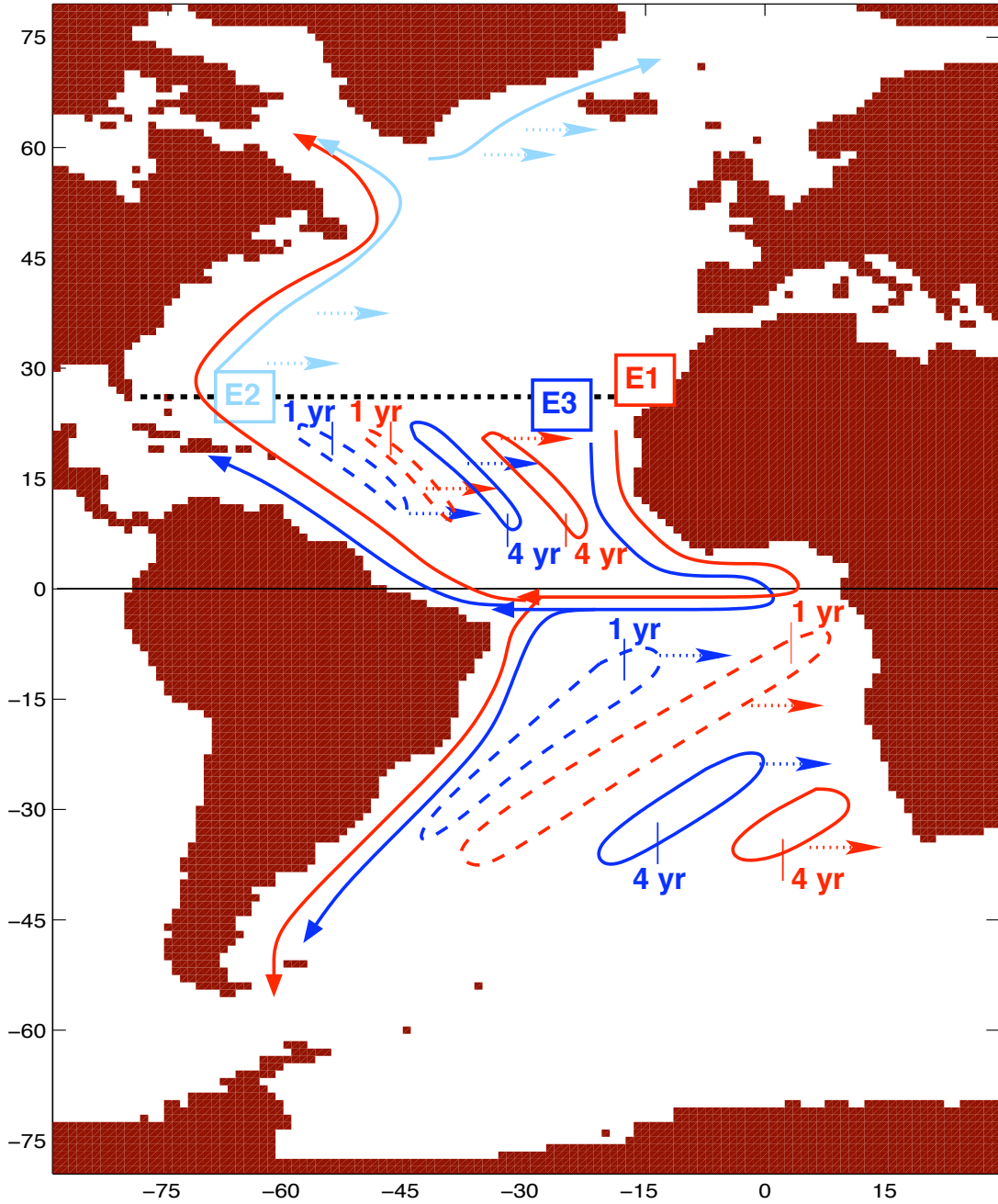


Figure 3: A schematic of dual Kelvin waves (lines) and dual Rossby waves (contours and dotted arrows) propagating sensitivities from the 26N line backward in time. Color coding refers to different events discussed in the text ([E1]: red, [E2]: light blue, [E3]: dark blue. `fig:map-schematic`

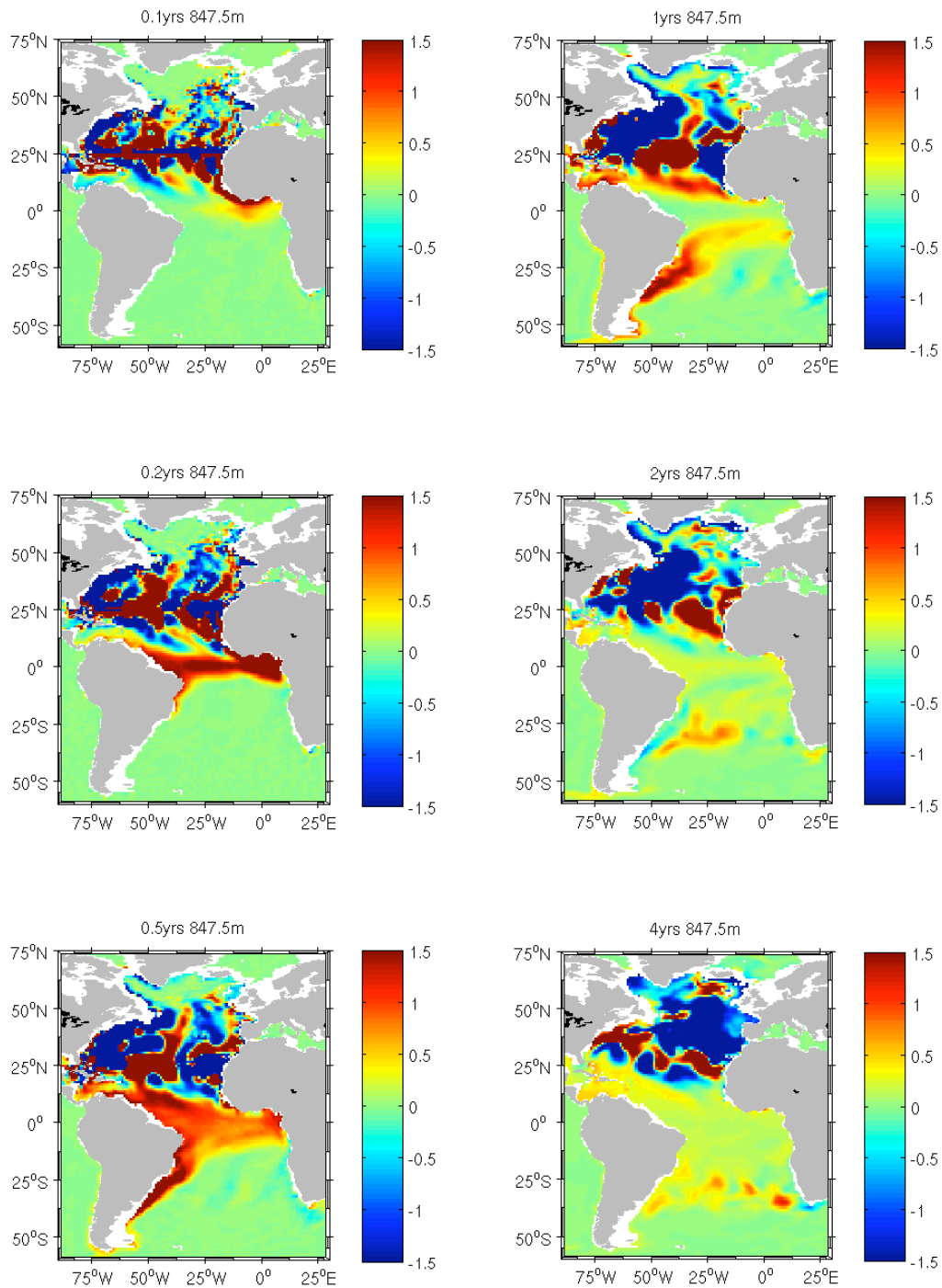
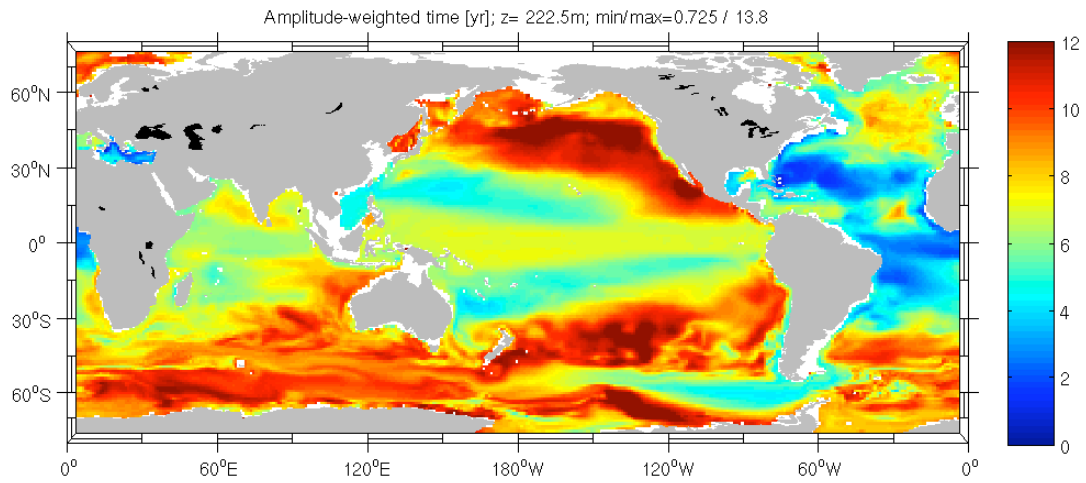
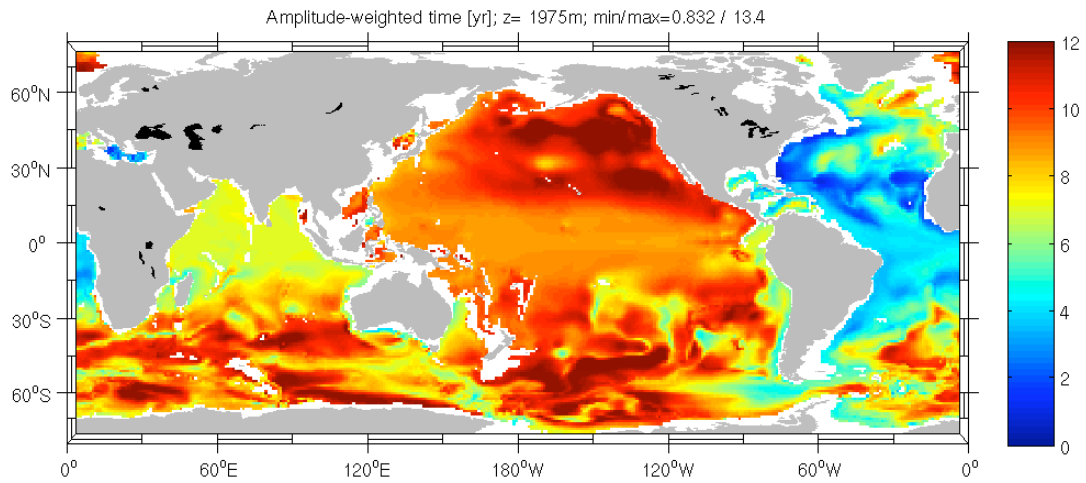


Figure 4: Same as Fig. 2, but at 847 m depth. fig:map-at1-0to4-k13



(a) 222 m depth



(b) 1975 m depth

Figure 5: Maps of mean times weighted by the amplitude of the normalized response fields, eqn. 5, for two different depth levels. Color scale refers to years (from 0 to 12). A small value in a certain region indicates fast dominant time scales of dynamical link between the region considered and 26N in the Atlantic.
fig:mean-time-maps

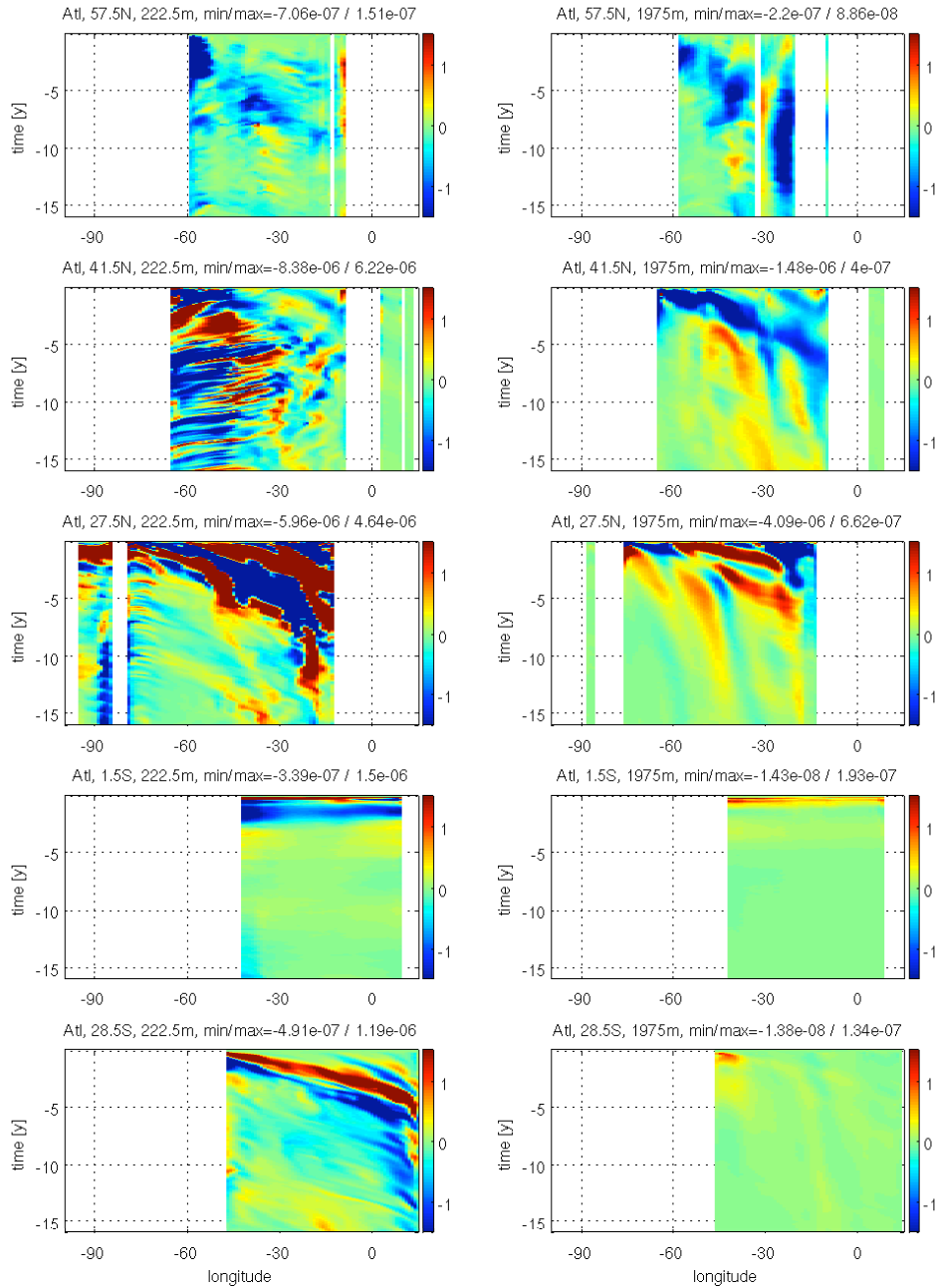


Figure 6: Normalized MVT responses plotted as a function of longitude and time at various latitudes (from top to bottom: 57.5N, 41.5N, 27.5N, 1.5S, 28.5S), and depths (left: 222 m, right 1975 m). The sensitivities were calculated via eqn. (4). The negative time axis reflects integration backwards of the adjoint model from the evaluation time of the MVT diagnostic ($t=0\text{yr}$). `fig:hovm-merid-moc-atl`

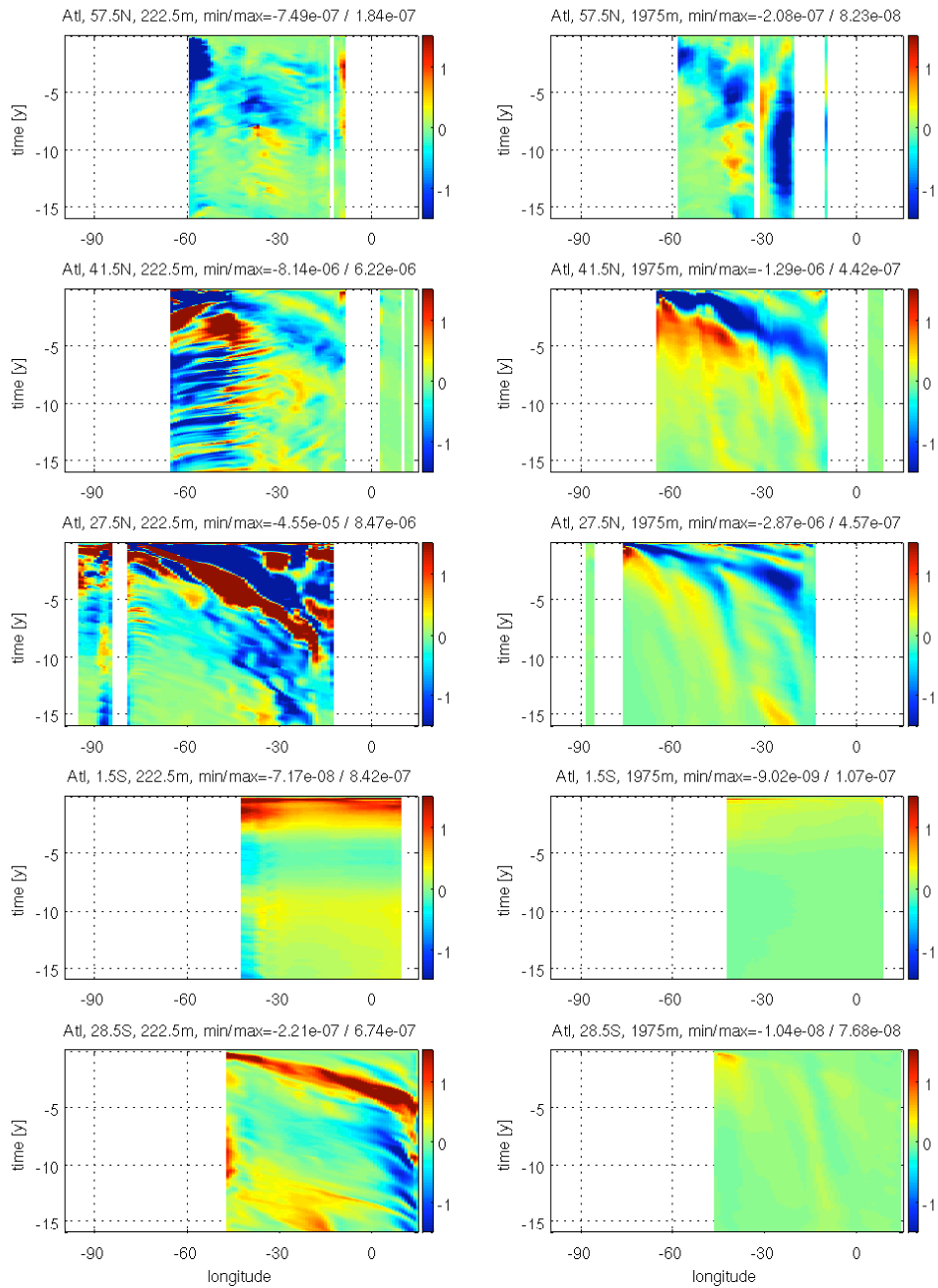


Figure 7: Same as Fig. 6, but for normalized MHT responses. `fig:hovm-merid-hf-atl`

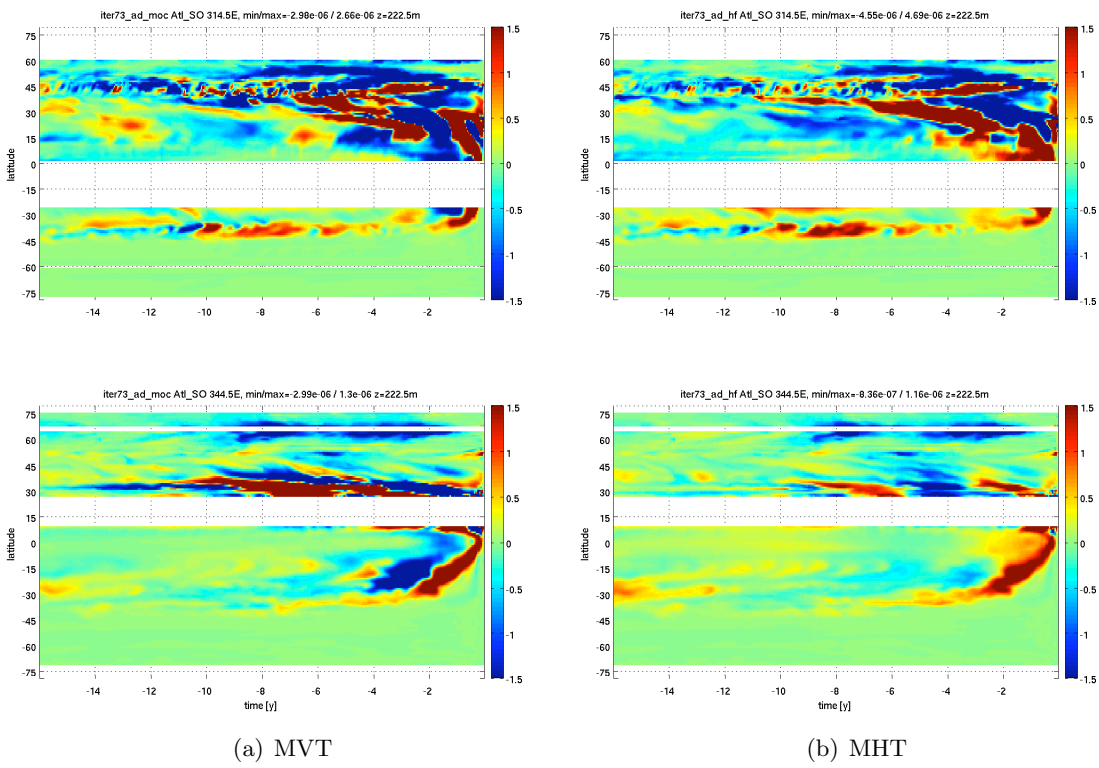


Figure 8: Normalized responses for MVT (left) and MHT (right) at 222 m depth at fixed longitudes 45°W (top) and 15°W (bottom), as function of time and latitude. `fig:zonal-point-at1`

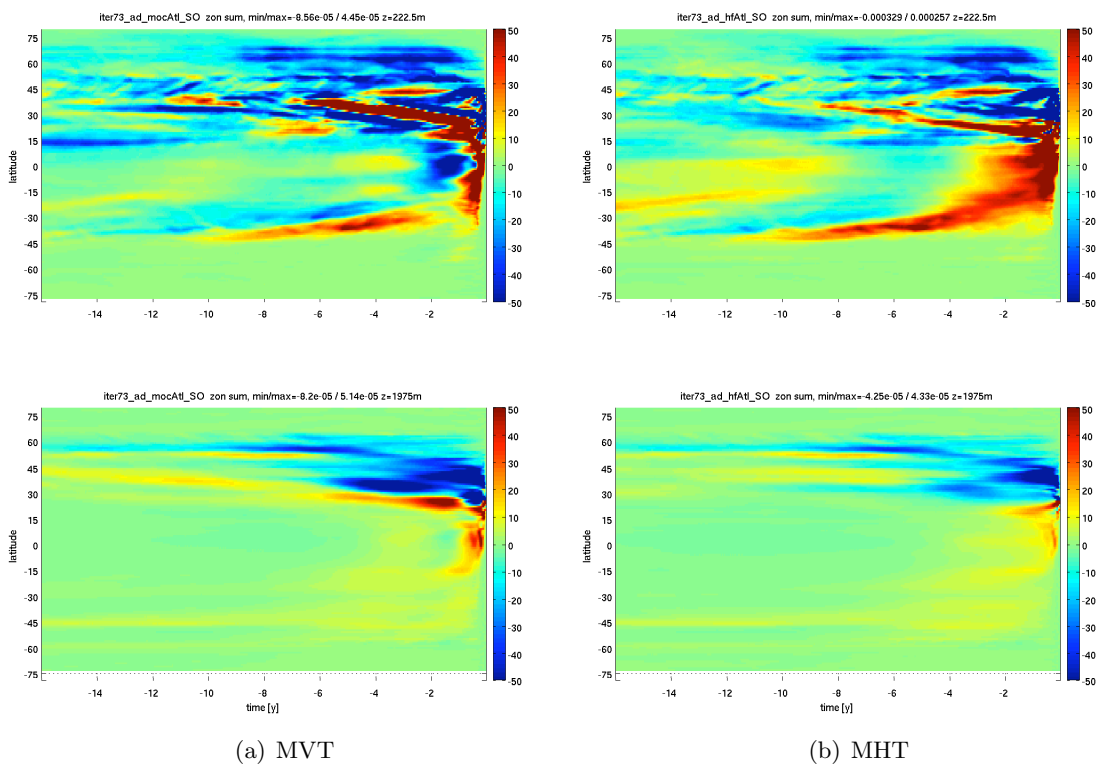


Figure 9: Same as Fig. 8, but for the zonally integrated sensitivities (rather than those at particular longitudes) in the Atlantic. fig:zonal-sums-atl

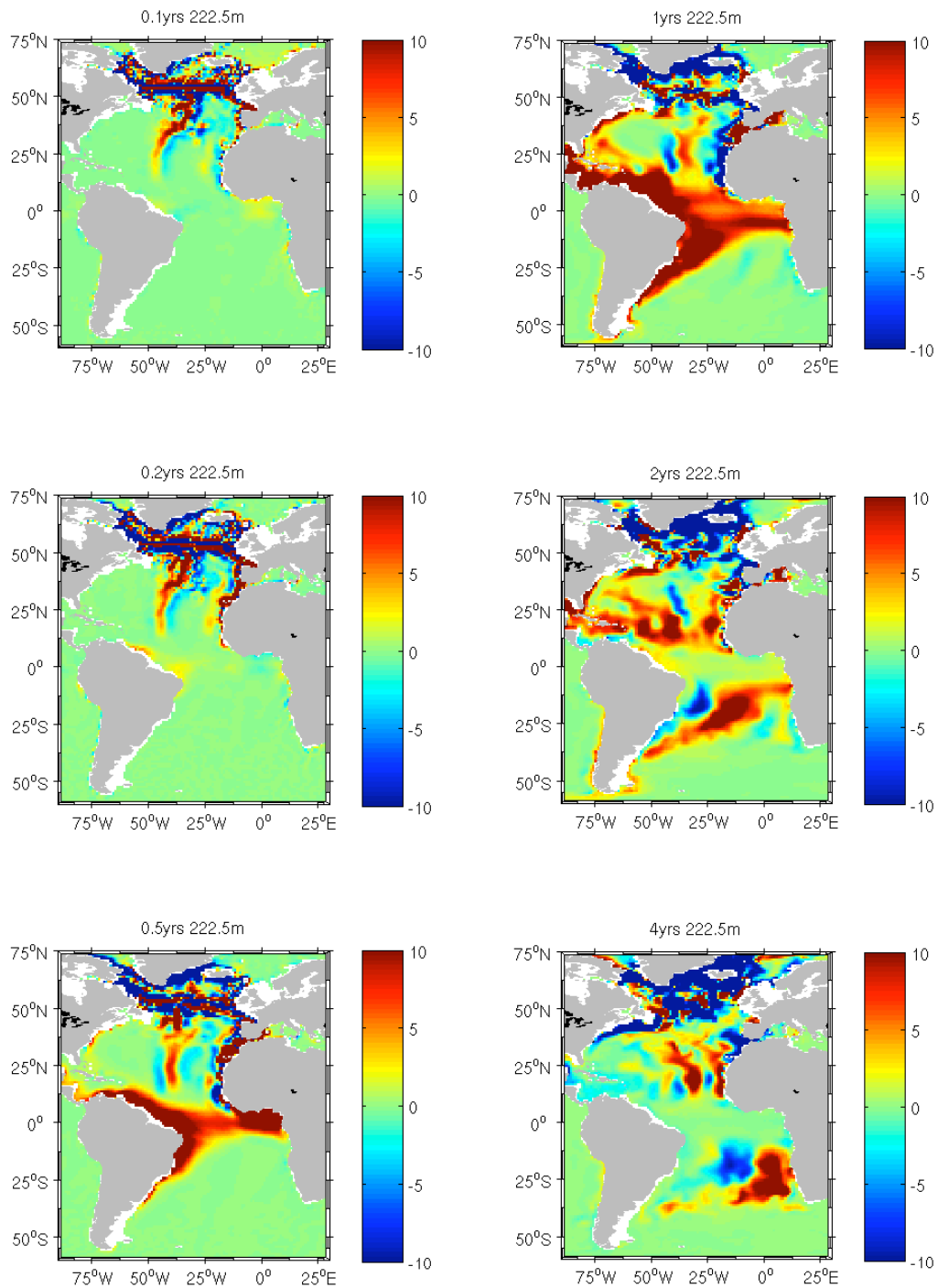
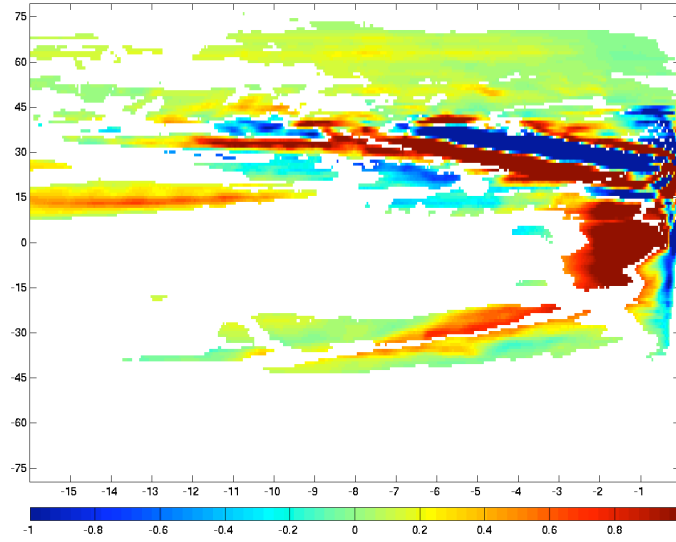
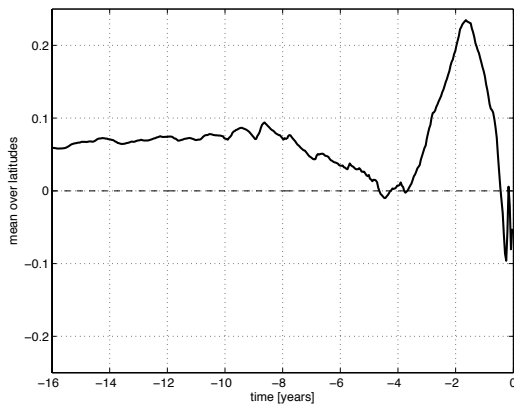


Figure 10: Maps of normalized temperature response fields of meridional volume transport, δJ_{MVT} , similar to Fig. 2, but for MVT at 48°N, in the Atlantic at 222 m depth, . Panels and units are as in Fig. 2.

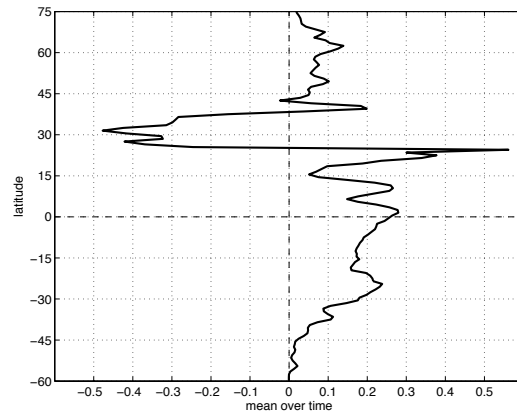
fig:map-spg-moc



(a)



(b)



(c)

Figure 11: (a): Latitude vs. time plot at 222 m depth levels of the difference $\frac{1}{\gamma} (\delta J_{MHT} - \delta J_{MVT})$ taken from zonally integrated sensitivities in Fig. 9, and with a range value of $\gamma = 5 \cdot 10^{-6}$. All signals for which the range of δJ_{MHT} itself is less than 20% of γ are suppressed to focus on sizable signals only. Taking the mean over latitudes or time of panel (a) produces condensed plots (b) and (c), respectively. `fig:diff-mht-mvt`

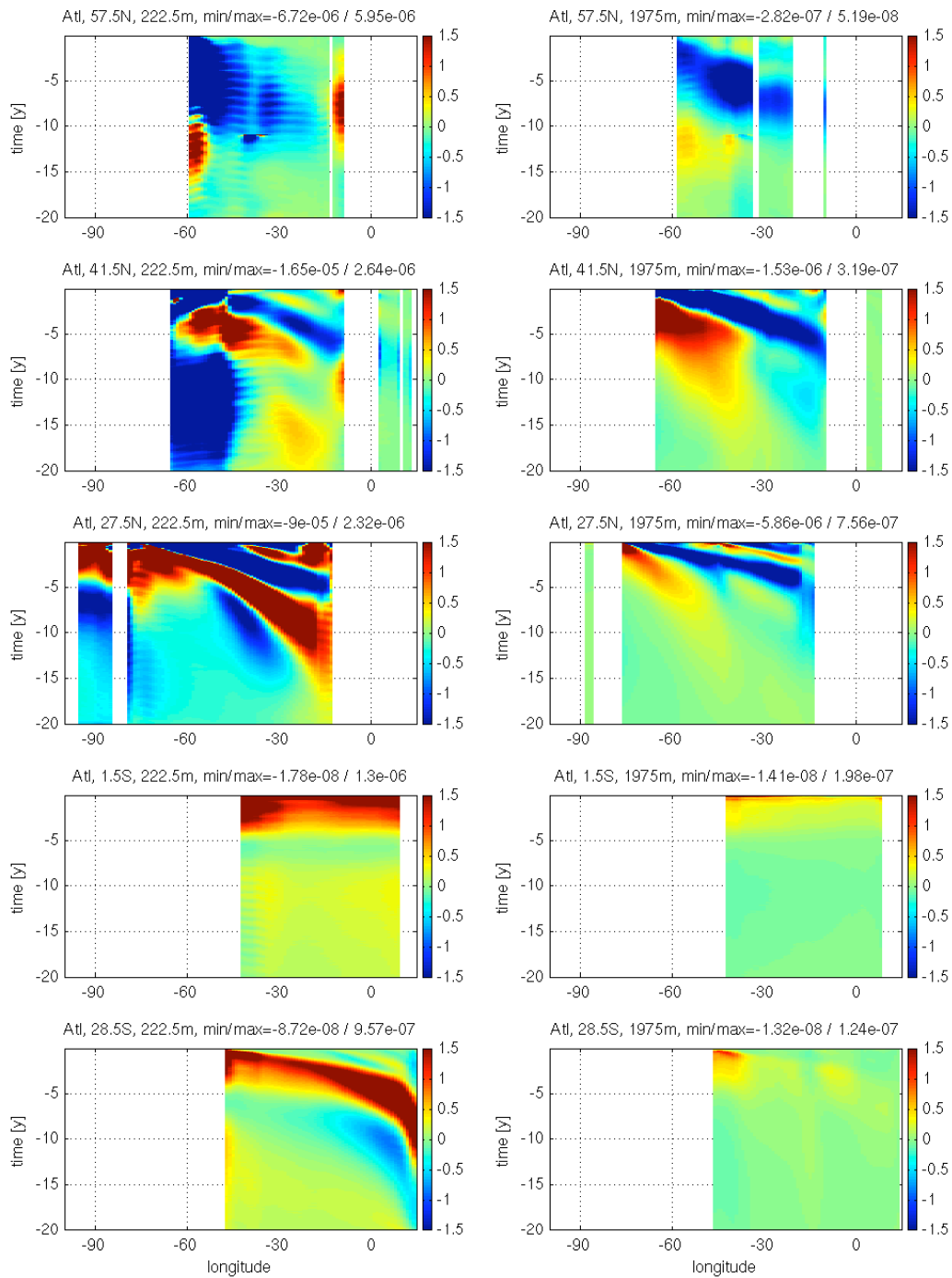


Figure 12: Same as Fig. 7, but computed from a non-optimized forward model trajectory, and going 20 years back in time. `fig:hovm-merid-hf-atl-nonoptim`

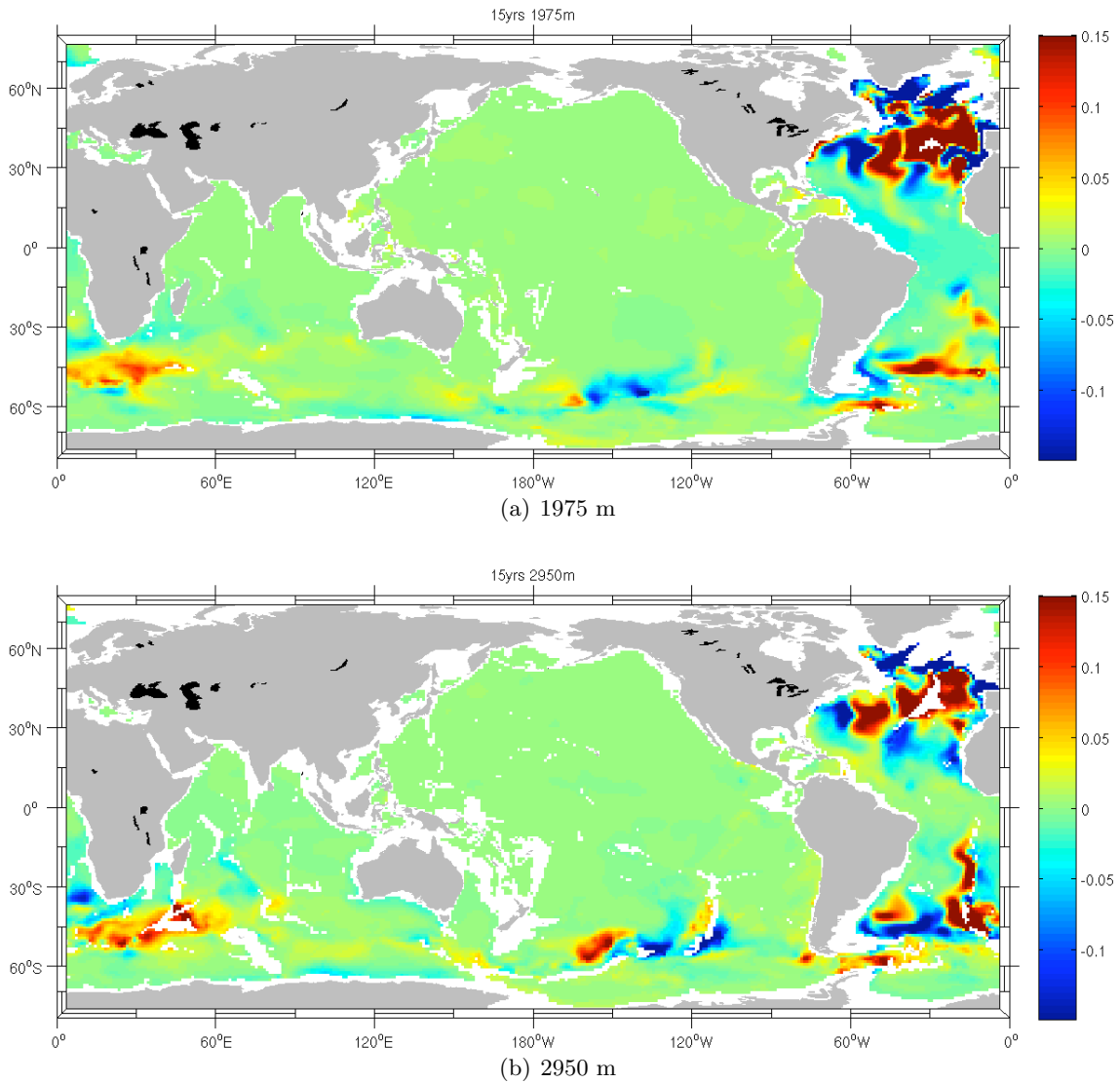


Figure 13: Normalized MVT response maps similar to those in Fig. 2, but now 15 years backward in time, at depth (left: 1975m, right 2950m), and mostly an order of magnitude smaller. While the overall influence on MVT thus diminishes, the area of influence extend beyond the Atlantic, with significant contributions from various parts of the Southern Ocean. `fig:map-deep-15yr`

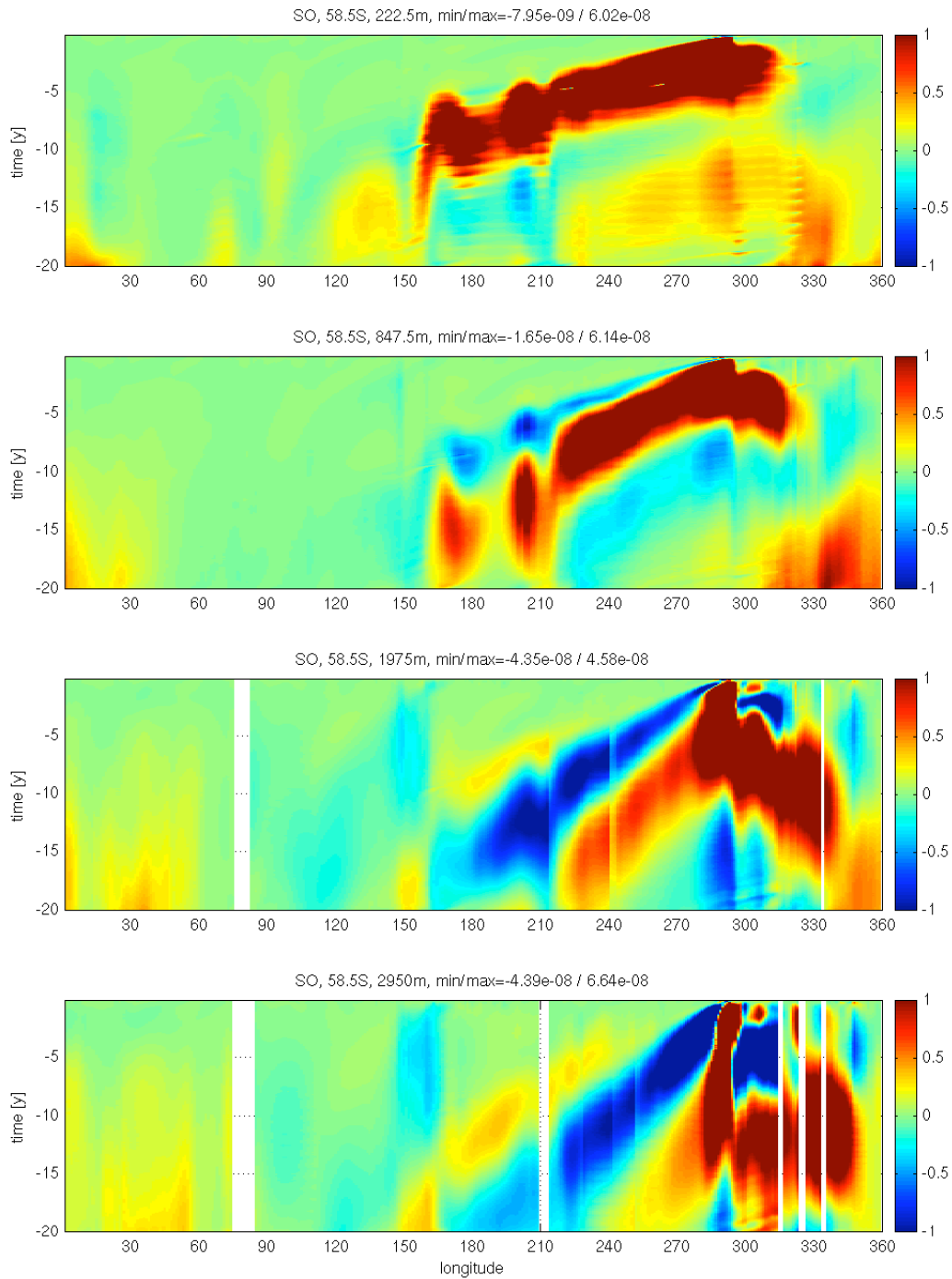


Figure 14: Meridional lines vs. time, similar to those in Fig. 12, but in the Southern Ocean at 58S and extended throughout the global latitude circle. Depth levels are, from top to bottom, 222m, 847m, 1975, and 2950m. A clear westward propagation (backward in time) is visible from the Atlantic to the Pacific basin (the connection occurring through the Drake Passage around 70W), whose speed is a function of depth (the increasing “tilt” in the panels from top to bottom corresponds to slower propagation).

fig:hovm-merid-so-222m

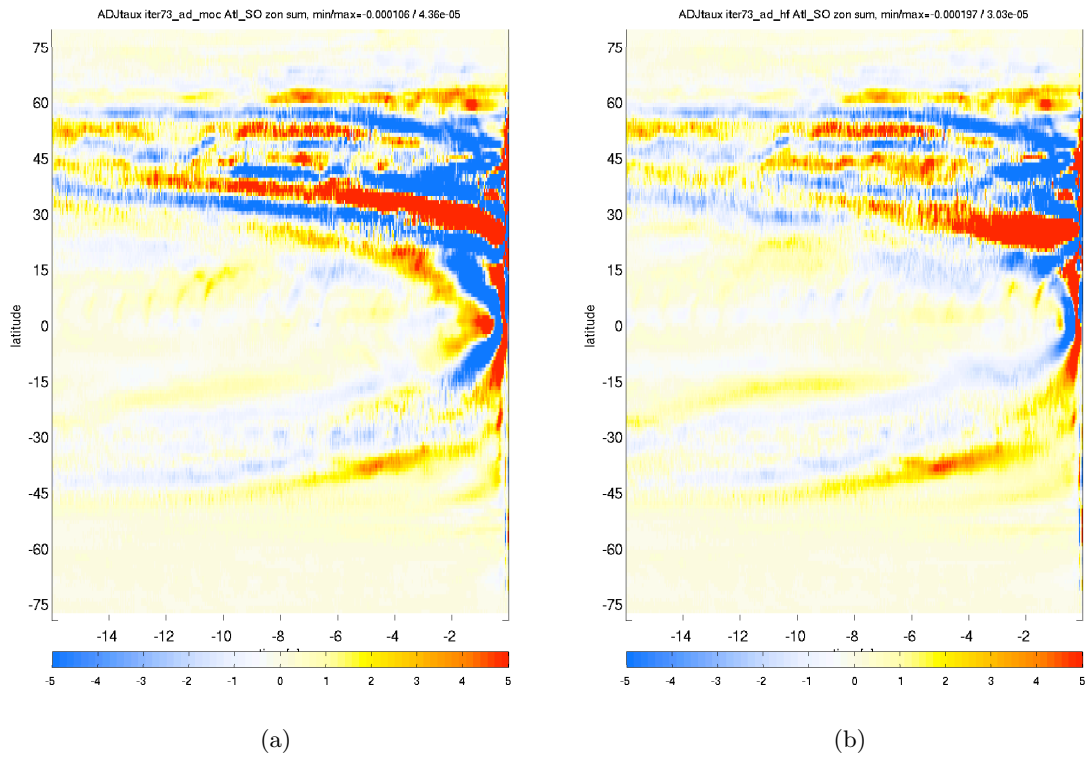


Figure 15: Zonally integrated normalized responses for MVT (a) and MHT (b) to zonal wind stress perturbations as function of time and latitude in the Atlantic (comparable to those of 222 m temperature responses, Fig. 9). `fig:taux-fields`

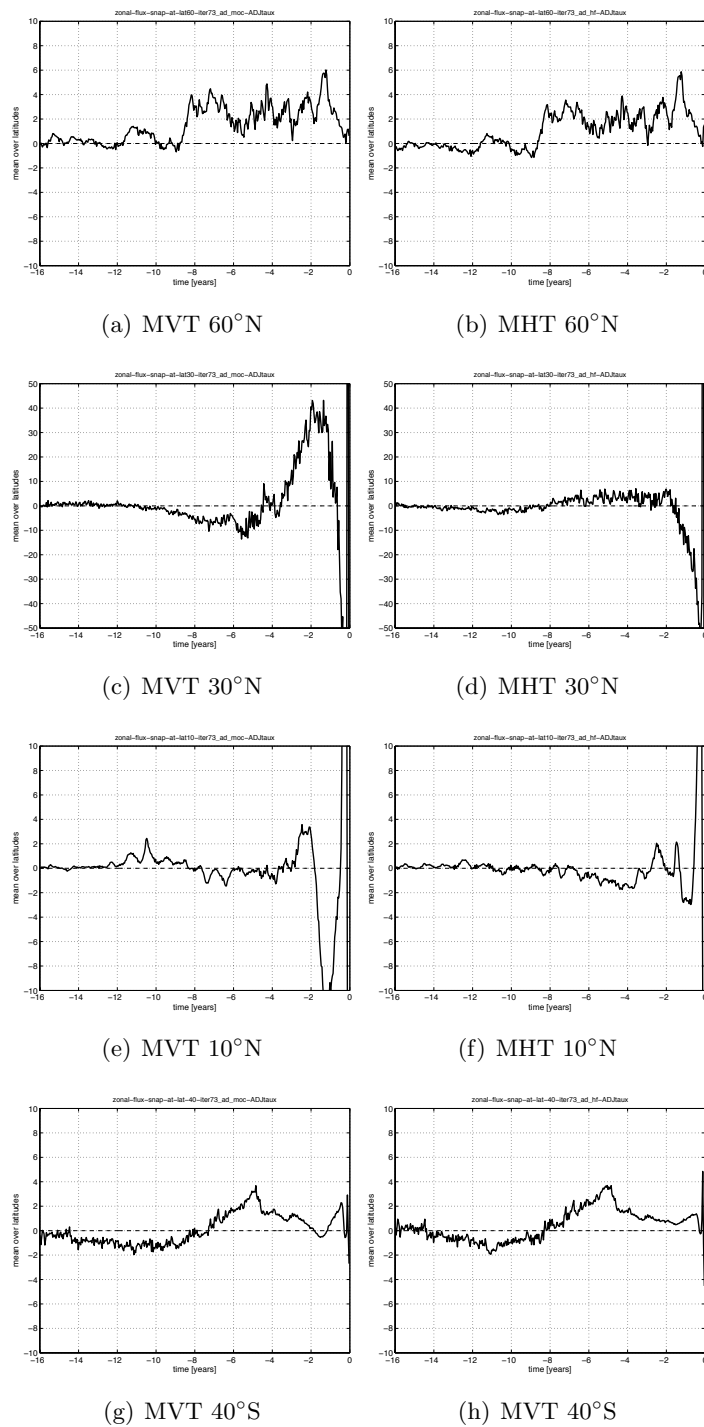


Figure 16: Time series of MVT (left) and MVT responses to zonal wind stress perturbations at various latitude sections, extracted from fields depicted in Fig. 15. `fig:taux-graphs`